# Immersion Sn Finish Processed on Ag Surface via Galvanic Reduction

**Chen Yu Wu**
National Central University
**Yi Xuan Lin**
National Central University
**Jyun Yang Wang**
National Central University
**Chia Hung Lee**
National Central University
**Chung Yu Chiu**
National Central University
**Ching Yu Yeh**
National Central University
**Bo Rong Huang**
National Central University
**Kuan Lin Fu**
National Central University
**Jui Sheng Chang**
National Central University
**ChengYi Liu** ( chengyiliuoem@gmail.com )
National Central University https://orcid.org/0000-0002-0930-2609

**Research Article**

**Keywords:** Electroless Ni, Immersion Ag, Immersion Sn, Galvanic reduction, Intermetallic compound (IMC), Thin film

**Posted Date:** March 22nd, 2021

**DOI:** https://doi.org/10.21203/rs.3.rs-308958/v1

**Version of Record:** A version of this preprint was published at Journal of Materials Science: Materials in Electronics on July 7th, 2021. See the published version at https://doi.org/10.1007/s10854-021-06306-6.

# Immersion Sn finish processed on Ag surface via galvanic reduction

C. Y. Wu, Y. X. Lin, J. Y. Wang, C. H. Lee, C. Y. Chiu, C. Y. Yeh, B. R. Huang, K. L. Fu, J. S. Chang, and C. Y. Liu

Department of Chemical Engineering and Materials Engineering,

National Central University, Jhong-Li, Taiwan 32001

## Abstract

Typically, Sn cannot be finished on Ni and Ag surfaces via the immersion process. In this work, through galvanic reaction, immersion Sn finish was processed on an immersion Ag finish coexisting with a Ni surface. Herein, the detailed mechanism of the reduction of $Sn^{2+}$ ions on the immersion Ag surface through galvanic reaction is reported. Through transmission electron microscopy and X-ray diffraction analysis, the uncommon $Ag_4Sn$ phase, instead of the common $Ag_3Sn$ phase, was confirmed to form during the Sn immersion of the Ag immersion layer. The $Ag_4Sn$ phase was found to form between the Ag grains in the immersion Sn layer. The mixed $Ag/Ag_4Sn$ structure in the immersion Sn layer can be explained by the galvanic reaction. The preferred formation of the $Ag_4Sn$ during the Sn immersion of the Ag immersion layer is discussed from the viewpoint of thermodynamics. The changes in the Gibbs free energy of the formation of the $Ag_3Sn$ and $Ag_4Sn$ phases were calculated as −3.67 and −8.89 kJ/mol, respectively. This confirms that the $Ag_4Sn$ phase is the favorable phase formed in the immersion Sn over the immersion Ag layer.

Keywords: Electroless Ni; Immersion Ag; Immersion Sn; Galvanic reduction; Intermetallic compound (IMC); Thin film

Corresponding author: chengyiliuoem@gmail.com

## 1. Introduction

Electroless Ni (EN) plating has been widely used as a surface finish in microelectronic packaging applications owing to its advantages of low cost, good corrosion resistance, and excellent mechanical properties of plated materials soldered with Pb-free solders [1-4]. A typical immersion Au layer is coated on the EN surface to preserve the solderable EN surface finish, and the composite surface is called the electroless Ni/immersion Au (ENIG) finish. The black pad, which occurs in the immersion Au deposition step, is a notable issue in ENIG [5]. Moreover, the Au immersion plating solution contains cyanide, which is harmful to the environment.

Many alternative surface finishes, such as Ag finish, have been studied to replace the immersion Au on the EN surface. Ag surface finishes have been widely used in electronic devices owing to their good conductivity and high reflectivity. However, Ag finishes easily sulfurize in the atmosphere, and Ag electrochemical migration is always a critical concern [6]. Immersion Sn finishes are cost effective and have high reliability and wettability with Pb-free solders [7]. Therefore, immersion Sn finish has been proposed on immersion Ag finish to prevent Ag sulfurization and reduce Ag migration. Moreover, potential Sn–Ag compound phase formed on the Ag surface finishes in the Sn immersion process has been reported to have excellent corrosion resistance and good resistance to the formation of Sn whiskers [8].

In this work, immersion Sn was processed on an Ag surface using a special galvanic reduction method. $Sn^{2+}$ ions were reduced by the electrons transferred from the Ni substrate on which the Ag surface was deposited. Furthermore, $Ag_3Sn$ is the typical phase formed in the Ag–Sn reaction couple, and it has been extensively studied [9-11]. In the Sn–Ag alloy electroplating process, $Ag_3Sn$ is the only phase formed on a Ni plating substrate [12]. Rossi et al. showed that in a Sn/Ag submicro-bilayer prepared via thermal evaporation, only the $Ag_3Sn$ phase was observed in the Sn/Ag bilayers [13].

Further, Wronkowska et al. showed that the $Ag_3Sn$ phase was formed in a Sn–Ag ultrathin bilayer (~70-nm thickness) prepared via thermal evaporation [14]. In the galvanic Sn reduction process employed in this work, an unusual intermetallic $Ag_4Sn$ compound was formed. The detailed mechanism of the reduction of $Sn^{2+}$ ions on the immersion Ag layer is proposed. In addition, the formation of the $Ag_4Sn$ phase during the Sn immersion of the immersion Ag layer is discussed from the viewpoint of thermodynamics.

## 2. Experimental procedures

The process of electroless Ni/immersion Ag (ENIS) deposition on a Cu-plated FR-4 substrate was studied in this work. The EN preparation is described as follows: First, 2-$cm^2$ Cu-plated FR-4 substrates were soaked in an acid detergent (ACL-007) for 5 min to degrease the possible organic contamination on the Cu surface. The degreased Cu surface was cleaned with 3,3′-dithiobis-1-propanesulfonic acid solution for 2 min. The Cu surface oxides were removed by immersing the Cu substrates in 10-vol.% $H_2SO_4$ etching solution at room temperature for 1 min. A Pd activation layer was deposited on the Cu substrate through the immersion process. Then, a 3-μm-thick EN layer was plated on the Pd activation layer at 82°C for 30 min (P content was approximately 9–10 wt.%), as seen in Fig. 1(a).

After the abovementioned EN-plating process, the immersion Ag layer was processed on the blank EN, as shown in Fig. 1(b). The Ag immersion process is described here. The EN/Cu substrates were rinsed with deionized water using an ultrasonic machine for 30 s and dried using $N_2$ gas purge. The EN/Cu substrates were then soaked in the immersion predipping solution for 10 s. Subsequently, the EN substrates were immersed in the Ag immersion plating solution at 50°C for 90 s. A 55-nm-thick immersion Ag layer was plated on the Ni(P) layer (Fig. 1b; the combined layer

is referred to as ENIS). The partial-immersion Ag layer on the EN substrate was removed via a simple lithographic process (Fig. 1c). For this particular substrate structure, the Ag and EN surfaces were exposed (the EN/ENIS composite surface is denoted as EN-ENIS surface in the following discussion).

Immersion Sn finish was processed on both ENIS and EN-ENIS substrates by immersing the substrates in Sn solution at 80°C for 1, 3, 5, and 10 min. The surface morphologies of the immersion Sn on the ENIS and EN-ENIS surfaces were obtained using a cold-field-emission scanning electron microscope. The compositions of the immersion Sn processed on the ENIS and EN-ENIS surfaces were analyzed via energy-dispersive X-ray spectroscopy (EDS). The cross sections of the immersion Sn layer on the ENIS and EN-ENIS surfaces were imaged using the focused ion beam (FIB) technique and high-resolution transmission electron microscopy (HR-TEM). The phase of the immersion Sn layers was further defined via X-ray diffraction (XRD, Cu $K_\alpha$ radiation source) and HR-TEM selected-area diffraction. The potential difference between the EN and immersion Ag in the Sn plating solution was measured using a potentiostat.

## 3. Results and discussion

### 3.1 Immersion Ag on EN surface

A typical nodular surface was observed on the EN surface (Fig. 2a). Figure 2(b) shows the surface morphology of the immersion Ag layer deposited on the EN layer with a deposition time of 15 s. The immersion Ag did not occur as a smooth layer on the EN surface. Ag particles (~15-nm diameter) were observed on the EN surface (Fig. 2b). As shown in Fig. 2(c), for an immersion time of 45 s, Ag particles on the EN surface were larger. The average size of the Ag particles was approximately 60 nm for an immersion time of 45 s. The Ag particles coalesced to form larger Ag particles. The

average size of the Ag particles increased to approximately 100 nm after an immersion time of 90 s, as shown in Fig. 2(d).

### 3.2 Immersion Sn over immersion Ag layer on ENIS and EN-ENIS

Figure 3 shows the scanning electron microscopy (SEM) images of the EN and ENIS surfaces after the Sn immersion process at 80°C for 1 min. No immersion Sn occurred on the EN surface (Fig. 3a). Instead, tiny pinholes caused by the corrosion in the Sn immersion solution formed on the nodules and grain boundaries of the EN substrate. In the case of the ENIS surface (Fig. 3b), the morphology of the Ag particles on the ENIS surface did not change after the Sn immersion process, thereby implying that Sn was not plated on the ENIS surface.

Figure 4 shows the SEM images of the immersion Sn on the EN-ENIS surface immersed in Sn solution for 1, 3, 5, and 10 min. The EN-ENIS surface comprised both EN and ENIS surfaces. Again, no immersion Sn layer was observed on the EN surface after the Sn immersion process, whereas a thin Sn layer occurred on the immersion Ag layer on the ENIS surface (Fig. 4a). As shown in Fig. 4(a), the immersion Sn layer exhibited a meshed structure. Pores (~80 nm) occurred on the surface of the immersion Sn layer for an immersion time of 1 min. After a 3-min immersion, the pores of the meshed immersion Sn layer grew larger and the immersion Sn layer exhibited a worm-like network structure, which did not change much with the increase in the Sn immersion time (5 and 10 min) (Fig. 4c and d).

Figure 5(a) shows the SEM image of the interface between the EN and ENIS surfaces. Figures 5(b) and 5(c) show the EDS mappings of the Ag and Sn on the EN-ENIS surface after the Sn immersion process, respectively. As shown in Fig. 5(c), Sn signals appeared on the ENIS surface but not on the EN surface. Again, this indicates that the immersion Sn could only be plated on the immersion Ag layer on the ENIS

surface. Thus, it can be concluded that the immersion Sn can only be plated on the immersion Ag surface coexisting with the EN surface. Figure 6 shows the FIB cross-sectional images of the immersion Sn on the EN-ENIS surface for 0, 1, 3, 5, and 10 min. The Pt layer on top of the immersion Ag layer was for protection in the FIB process. The FIB cross-sectional image (Fig. 6a) shows the morphology of the Ag clusters. Overall, the initial immersion Ag layer was continuous. Following the Sn immersion process, the immersion Sn/Ag layer exhibited discontinuities, as indicated by white arrows in Fig. 6(b–e). The discontinuities correspond to the pores in the worm-like network surface morphology of the immersion Sn/Ag (Fig. 4c and d).

As shown in the FIB cross-sectional images in Fig. 6(b–d), the immersion Sn plating on the immersion Ag layer cannot be distinguished from the initial immersion Ag layer; the combined layer is denoted as immersion Sn/Ag in the discussion that follows. The total thickness of the immersion Sn/Ag layer on the EN-ENIS surface was measured using Optimas software with FIB cross-sectional images. Figure 7 shows the thickness of the immersion Sn/Ag layer over the Sn immersion time. The thickness of the immersion Sn/Ag layer decreased rapidly during the first 1 min of plating and stabilized thereafter.

### 3.3 Phase formation of immersion Sn over immersion Ag

The immersion Ag layer on the EN-ENIS surface before and after the Sn immersion process was analyzed via XRD. Figure 8 shows the XRD patterns on the immersion Ag layer on the EN-ENIS surface before and after the Sn immersion process. The XRD patterns show a clear (111) Ag diffraction plane (Fig. 8a and b). Two additional peaks at the 2θ values of 37.59 and 39.80 existed in the XRD patterns of the immersion Sn/Ag layer on the EN-ENIS surface (Fig. 8a). The diffraction peak at 39.80 matches with the (011) plane of $Ag_4Sn$. The diffraction peak at 37.59 could be either the (200) plane of

$Ag_3Sn$ or the (002) plane of $Ag_4Sn$. The XRD results imply that the phase formed in the immersion Sn/Ag layer comprised the Ag phase and Sn–Ag compound phase ($Ag_3Sn$ or $Ag_4Sn$).

Based on the position of (111) Ag peaks in Figs. 8(a) and 8(b), the lattice parameter of the Ag phase in the immersion Ag layer (before the Sn immersion process) and immersion Sn/Ag layer (after the Sn immersion process) was calculated as 4.0864 Å and 4.0916 Å, respectively [15]. Moreover, with the increase in the immersion Sn amount, the lattice constant of the Ag phase in the immersion Sn/Ag layer increased. This increase in the lattice parameter can be attributed to the Sn dissolution in the Ag phase in the immersion Sn/Ag layer. Karakaya et al. studied the variation in the Ag lattice parameter with respect to Sn solubility. The solubility limit of Sn in Ag is approximately 11.5 at.%, which corresponds to the Ag lattice parameter of 4.132 Å [15-16]. Based on Karakaya's results, the calculated lattice parameter (4.0916 Å) of the Ag phase in the immersion Sn/Ag layer corresponds to the Sn solubility (1.31 at.%) in the Ag phase in the immersion Sn/Ag layer.

Furthermore, the immersion Sn/Ag layer was subjected to TEM selected-area diffraction analysis (SADA); the results are indicated with the red circle in Fig. 9(a). Two phases, Ag and $Ag_4Sn$, were confirmed via TEM SADA (Fig. 9b). Figure 10 shows the enlarged HR-TEM images of the immersion Sn/Ag layer. A granular structure can be observed in the enlarged image in Fig. 10(b). The possible d-spacing in each grain area can be estimated by the atomic resolution in the grains shown in Fig. 10(b). The d-spacing values for the three grains shown in Fig. 10(b) were calculated as 2.358, 2.391, and 2.263 Å. The calculated d-spacing (2.358 Å) matches the d-spacing of the (111) plane of the Ag phase, which is labeled as a Ag phase in Fig. 10(b). Moreover, the calculated d-spacing of 2.391 and 2.263 Å correspond to the (002) and (011) planes of $Ag_4Sn$, respectively. The phases of the grains in the immersion Sn/Ag layer were

determined and are marked in Fig. 10(b). Figure 10(b) indicates that the $Ag_4Sn$ phase was formed between Ag grains in the immersion Sn/Ag layer.

Based on these XRD patterns, HR-TEM images, and SADA results, it can be concluded that as the immersion Sn was plated on the immersion Ag layer, the $Ag_4Sn$ phase—instead of the common $Ag_3Sn$ phase—was formed between the Sn and Ag reaction couples.

The effective heat of formation (EHF) model has been proposed to predict the phase formation in the Sn–Ag reaction [17-18]. The EHF model can be used to calculate the formation heat of the Sn–Ag compound phase, $\Delta Hf^*$, as a function of the Ag concentration, as shown in Eq. (1):

$$\Delta \boldsymbol{Hf}^* = \Delta \boldsymbol{Hf}^\circ \times \frac{\boldsymbol{c}_{\boldsymbol{Ag}}^{\boldsymbol{I}}}{\boldsymbol{c}_{\boldsymbol{Ag}}^\circ}, \quad (1)$$

where $\Delta Hf^\circ$ is the standard heat of formation, $c^I_{Ag}$ is the actual average concentration of the limiting element (Ag) in the Sn–Ag layer, and $c^\circ_{Ag}$ is the theoretical concentration of the limiting element (Ag) in the Sn–Ag compound phase. Flandorfer et al. defined the $\Delta Hf^\circ$ values of the $Ag_3Sn$ and $Ag_4Sn$ compound phases as −4.2 and −2.8 kJ/mol, respectively [19], and the theoretical concentrations of the limiting element (Ag) in the $Ag_3Sn$ phase and the $Ag_4Sn$ phase are 0.75 and 0.8 at.%, respectively. The actual average concentration of the limiting element (Ag), $c^I_{Ag}$, was measured as 0.655 at.% through X-ray photoelectron spectroscopy analysis. When the necessary parameters ($\Delta Hf^\circ$, $c^I_{Ag}$, and $c^\circ_{Ag}$) were substituted in Eq. (1), the $\Delta Hf^*$ values for forming the $Ag_3Sn$ phase and $Ag_4Sn$ phase were obtained as −3.67 and −2.29 kJ/mol, respectively. The $\Delta Hf^*$ for forming the $Ag_3Sn$ phase is more negative than that for forming the $Ag_4Sn$ phase; therefore, based on the above calculation from the EHF model, the favorable Sn–Ag phase formation during the Sn immersion process should be the $Ag_3Sn$ phase. The prediction from the EHF model does not match the actual

result in this work; that is, the $Ag_4Sn$ phase was formed during the Sn immersion of the immersion Ag layer. Note that the EHF model assumes an ideal stoichiometric composition for the phases involved in the prediction. Thus, the formation heat of the phases can solely be used to predict the favorable phase formation in the chemical reaction. The $Ag_4Sn$ formed in the immersion Sn/Ag layer can be a highly nonstoichiometric phase, which can tolerate a great amount of the Ag or Sn vacancy. Hence, the entropy should play a major role in the formation of the nonstoichiometric $Ag_4Sn$ phase in the immersion Sn/Ag layer. Next, the actual composition of the $Ag_4Sn$ phase formed in the immersion Sn/Ag layer was evaluated.

Ag and $Ag_4Sn$ are the two phases in the immersion Sn/Ag layer; therefore, the Sn amount ($W_{Sn}$ in weight) in the immersion Sn/Ag layer comprises the Sn amount dissolved in the Ag phase ($W_{Sn(Ag)}$ in weight) and the Sn amount in the $Ag_4Sn$ phase ($W_{Sn(Ag4Sn)}$ in weight), as given by Eq. (2). The notations in parentheses above and in the following discussion represent the phase formed; for example, the subscript in $W_{Sn(Ag)}$ means that Sn is in the Ag phase.

$$W_{Sn} = W_{Sn(Ag4Sn)} + W_{Sn(Ag)}. \quad (2)$$

Further, weight percentage is used for the terms in the following discussion. $W_{Sn/layer}$ is defined as the weight percentage of Sn in the immersion Sn/Ag layer, which is the total amount of Sn ($W_{Sn}$) divided by the total amount of the immersion Sn/Ag layer ($W_{layer}$). Similarly, $W_{Sn(Ag4Sn)/layer}$ and $W_{Sn(Ag)/layer}$ are the amounts of Sn in the $Ag_4Sn$ and Ag phases divided by the total amount of the immersion Sn/Ag layer ($W_{layer}$), respectively. Thus, Eq. (2) can be rewritten as Eq. (3):

$$W_{Sn/layer} = W_{Sn(Ag4Sn)/layer} + W_{Sn(Ag)/layer}. \quad (3)$$

The third term in Eq. (3) can be expressed as the product of the Sn solubility in the Ag phase ($S_{Sn/(Ag)}$) in the immersion Sn/Ag layer and the weight percentage of the Ag phase in the immersion Sn/Ag layer ($W_{(Ag)/layer}$), i.e., $S_{Sn/(Ag)} \times W_{(Ag)/layer}$. Then, Eq. (3) can be

further expressed as Eq. (4):

$$W_{Sn(Ag4Sn)/layer} = W_{Sn/layer} - (S_{Sn/(Ag)} \times W_{(Ag)/layer}). \quad (4)$$

The Sn solubility in the Ag phase ($S_{Sn/(Ag)}$) in the immersion Sn/Ag layer has been previously determined as 1.44 wt.%. The overall Sn concentration ($W_{Sn/layer}$) in the immersion Sn/Ag layer was determined as 3.31 wt.% via TEM-EDS. Thus, if the weight percentage of the Ag phase in the immersion Sn/Ag layer ($W_{(Ag)/layer}$) is known, the term ($W_{Sn(Ag4Sn)/layer}$) in Eq. (4) can be calculated.

The weight percentages of the Ag phase ($W_{(Ag)/layer}$) and the $Ag_4Sn$ phase ($W_{(Ag4Sn)/layer}$) in the immersion Sn/Ag layer can be calculated using the XRD peak intensity ratio method (XRD RIR) using Eq. (5): [20]

$$W_{(Ag)/layer} = \frac{I_{Ag}}{I_{Ag} + \frac{I_{Ag_4Sn}}{K_{Ag}^{Ag_4Sn}}}, \quad (5)$$

where $I$ is the diffraction peak intensity of the corresponding phase and $K$ is the diffraction peak intensity ratio between the specific phases (Ag and $Ag_4Sn$ in this work) and the reference phase (typically, α-$Al_2O_3$) with a 1:1 weight ratio; here, $K_{Ag}$ and $K_{Ag4Sn}$ are 5.2 and 17.0, respectively, from the JCPDS database, and $K_{Ag}^{Ag4Sn}$ is the ratio of $K_{Ag4Sn}$ to $K_{Ag}$. Based on the rule of the RIR method, $I_{Ag}$ and $I_{Ag4Sn}$ are respectively taken as the peak intensities of the (111) Ag diffraction and (002) $Ag_4Sn$ diffraction shown in Fig. 8(b).

By inserting all required parameters in Eq. (5), $W_{(Ag)/layer}$ and $W_{(Ag4Sn)/layer}$ were calculated as 88.65 and 11.35 wt.%, respectively. By inserting the obtained $W_{(Ag)/layer}$ in Eq. (4), the $W_{Sn(Ag4Sn)/layer}$ was calculated as 2.04 wt.%.

Moreover, the actual Ag weight percentage in the $Ag_4Sn$ phase ($W_{Ag(Ag4Sn)/layer}$) can be expressed as Eq. (6):

$$W_{Ag(Ag4Sn)/layer} = W_{(Ag4Sn)/layer} - W_{Sn(Ag4Sn)/layer}. \quad (6)$$

The $W_{(Ag4Sn)/layer}$ and $W_{Sn(Ag4Sn)/layer}$ in Eq. (6) were determined as 11.35 and 2.04 wt.%. Thus, the $W_{Ag(Ag4Sn)/layer}$ value can be determined as 9.31 wt.%. The weight percentage of Sn in the $Ag_4Sn$ phase ($W_{Sn/(Ag4Sn)}$) can be calculated by dividing $W_{Sn(Ag4Sn)/layer}$ by $W_{(Ag4Sn)/layer}$. The values of $W_{Sn/(Ag4Sn)}$ and $W_{Ag/(Ag4Sn)}$ were determined as 17.98 and 82.02 wt.%, respectively. The atomic concentrations of Sn ($X_{Sn/(Ag4Sn)}$) and Ag ($X_{Ag/(Ag4Sn)}$) in the $Ag_4Sn$ phase were converted based on the obtained $W_{Sn/(Ag4Sn)}$ and $W_{Ag/(Ag4Sn)}$. The values of Sn ($X_{Sn/(Ag4Sn)}$) and Ag ($X_{Ag/(Ag4Sn)}$) in the $Ag_4Sn$ phase were 16.60 and 83.40 at.%, respectively. The obtained atomic percentage of the $Ag_4Sn$ phase shows that the $Ag_4Sn$ phase in the immersion Sn/Ag layer is nonstoichiometric.

The entropy change ($\Delta S$) of the formation of the nonstoichiometric $Ag_4Sn$ phase in the immersion Sn/Ag layer can be estimated using Eq. (7):

$$\Delta S = -nR(X_{Sn/(Ag4Sn)} \ln X_{Sn/(Ag4Sn)} + X_{Ag/(Ag4Sn)} \ln X_{Ag/(Ag4Sn)}). \quad (7)$$

With the obtained atomic concentrations of Sn ($X_{Sn/(Ag4Sn)}$) and Ag ($X_{Ag/(Ag4Sn)}$) in the $Ag_4Sn$ phase, the contribution of entropy changes of the $Ag_4Sn$ phase formation was calculated as −6.60 kJ/mol using Eq. (7). Based on the study by Abbott et. al, the $Ag_3Sn$ phase can typically be considered a perfect stoichiometric orthorhombic structure [21]. Therefore, the entropy change of the $Ag_3Sn$ phase formation can be neglected in the above calculation. Thus, using the expression of Gibbs free energy, the changes in the Gibbs free energy of the formation of the $Ag_3Sn$ and $Ag_4Sn$ phases were calculated as −3.67 and −8.89 kJ/mol, respectively. This confirms that the $Ag_4Sn$ phase is the favorable phase formed in the immersion Sn/Ag layer.

### 3.4 Galvanic cell and formation of Ag/$Ag_4Sn$ mixing layer

As seen in Fig. 11, during the Sn immersion process, a galvanic cell forms between the immersion Ag layer and EN substrate in the immersion Sn plating solution. The EN layer acts as the anode, producing electrons for the reduction of the $Sn^{2+}$ ions on the

cathodic Ag layer. The detailed process is described here. First, electrons are produced owing to the Ni oxidation at the anode. The released electrons move to the Ag cathode surface. The $Sn^{2+}$ ions in the plating solution receive the electrons and reduce to Sn atoms on the Ag surface. The open-circuit potential between the EN and immersion Ag layer in the immersion Sn plating solution was measured as 0.376 V using a potentiostat. The change in the Gibbs free energy of the redox reaction can be calculated using Eq. (8):

$$\Delta G = -nFE. \quad (8)$$

where $n$ is the number of moles of $e^-$ for the redox reaction, $F$ is Faraday's constant (96,485 C/mol), and $E$ is the potential difference of the reaction cell. The Gibbs free energy value ($\Delta G$) of the redox reaction was calculated as −72.56 kJ. The negative $\Delta G$ value means that the galvanic reaction between the EN layer and immersion Ag layer was a spontaneous reaction.

Methanesulfonic acid (MSA), which is the main additive in the immersion Sn plating solution, can prevent stannous methanesulfonate (the $Sn^{2+}$ ion source) from hydrolyzing. The SEM image in Fig. 12 shows a tilted view of the Ag clusters. Moreover, based on the image of Fig. 6(a), the cross-section of the immersion Ag layer can be sketched as Fig. 13(a). Hence, in the Sn immersion process, the MSA in the Sn immersion solution corrodes the boundaries among Ag clusters. Consequently, the Ni surface between Ag grains gets exposed, as shown in Fig. 13(b). As shown in Fig. 13(c), the exposed Ni surface releases electrons for the reduction of $Sn^{2+}$ ions and the $Sn^{2+}$ ions are reduced on both sides of the Ag clusters. The reduced Sn atoms react with the adjacent Ag grains with solid-state interdiffusion, as seen in Fig. 13(d). It has been reported that Ag solutes reside in the interstitial sites in Sn [22]. The Ag atoms diffuse to the Sn reduction phase and form a $Ag_4Sn$ compound phase. As a result, a $Ag/Ag_4Sn$ mixing layer is formed in the immersion Sn/Ag layer, as shown in the TEM images in

Fig. 10(b).

## 4. Conclusion

Immersion Ag on EN is a promising surface finish for modern electronic packaging. However, the Ag surface finish is subject to sulfurization, which is a major reliability issue. In this work, through galvanic reaction, immersion Sn was processed on immersion Ag finish coexisting with Ni surface. The $Sn^{2+}$ reduction mechanism on EN-ENIS can be explained by the galvanic reduction effect. A galvanic cell is formed between Ni(P) and Ag. The electrons are transported from the Ni side (cathode) to the Ag surface (anode). Then, the $Sn^{2+}$ ions are reduced and deposited on the Ag surface. Through TEM and XRD analysis, the $Ag_4Sn$ phase, instead of the common $Ag_3Sn$ phase, was confirmed to form in the Sn immersion process of the immersion Ag layer. The $Ag_4Sn$ phase formed between the Ag grains in the immersion Sn layer. Furthermore, the preferred formation of the $Ag_4Sn$ in the Sn immersion process of the immersion Ag layer was discussed from the viewpoint of thermodynamics. The changes in the Gibbs free energy of the formation of the $Ag_3Sn$ and $Ag_4Sn$ phases were calculated as −3.67 and −8.89 kJ/mol, respectively. This confirms that the $Ag_4Sn$ phase is the favorable phase formed in the immersion Sn over the immersion Ag layer.

**Data availability statement:**

The raw/processed data required to reproduce these findings cannot be shared at this time as the data also forms part of an ongoing study.

**Acknowledgements:**

We are grateful for the financial support from MOST 108-2221-E-008-045-MY3 and MOST 107-2221-E-008-042-MY3. The information consultancy of ENIG and

immersion Ag development trends provided by Taiwan Uyemura Co., Ltd. is greatly appreciated.

**Figure caption**

Figure 1. Schematic of (a) electroless EN substrate, (b) ENIS, and (c) EN-ENIS specimens

Figure 2. SEM images of (a) electroless EN, (b) 15-s-immersion Ag, (c) 45-s-immersion Ag, and (d) 90-s-immersion Ag

Figure 3. Immersion Sn on (a) EN substrate and (b) ENIS specimens

Figure 4. Immersion Sn with different plating times: (a) 1, (b) 3, (c) 5, and (d) 10 min

Figure 5. (a) SEM image of the interface between EN and ENIS, and EDS mapping of the selected region showing elemental distribution of (b) Ag and (c) Sn

Figure 6. Cross-section of the metallic layer with different Sn plating times: (a) as-plated Ag; and immersion Sn plating time for (b) 1, (c) 3, (d) 5, and (e) 10 min

Figure 7. Variation in metallic layer thickness with immersion time

Figure 8. XRD diffraction pattern of (a) as-deposited immersion Ag layer and (b) metallic layer after immersion Sn layer

Figure 9. HR-TEM selected-area diffraction of metallic layer

Figure 10. HR-TEM image of metallic layer

Figure 11. Schematic of nanogalvanic cell formation in EN-ENIS with immersion Sn plating solution

Figure 12. SEM images of Ag clusters with tilt angle

Figure 13. Schematic of Sn diffusion into Ag clusters with $Ag_4Sn$ formation along Ag grain boundaries

**Table caption**

Table. 1 HR-TEM-EDS results of average chemical compositions at points 1–5 marked in Fig. 10

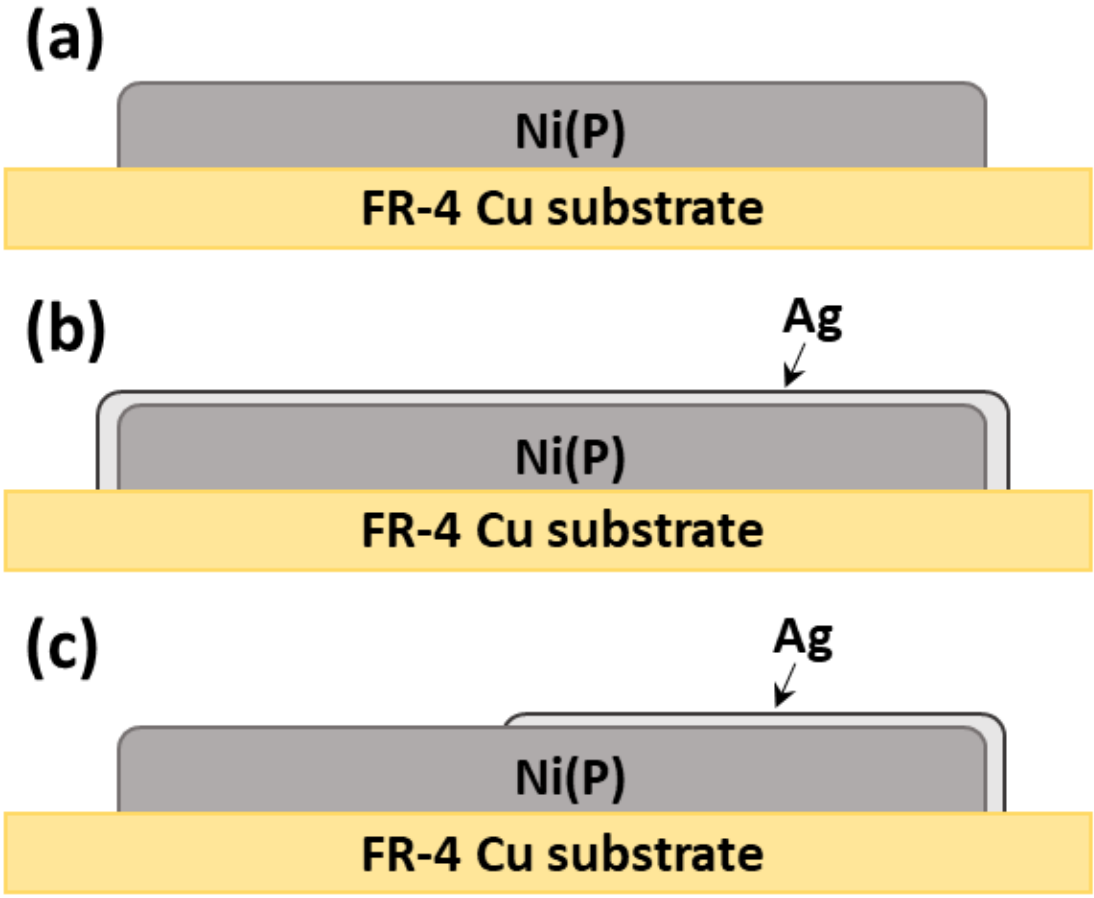
(a)
Ni(P)
FR-4 Cu substrate
(b)
Ag
Ni(P)
FR-4 Cu substrate
(c)
Ag
Ni(P)
FR-4 Cu substrate

Fig. 1

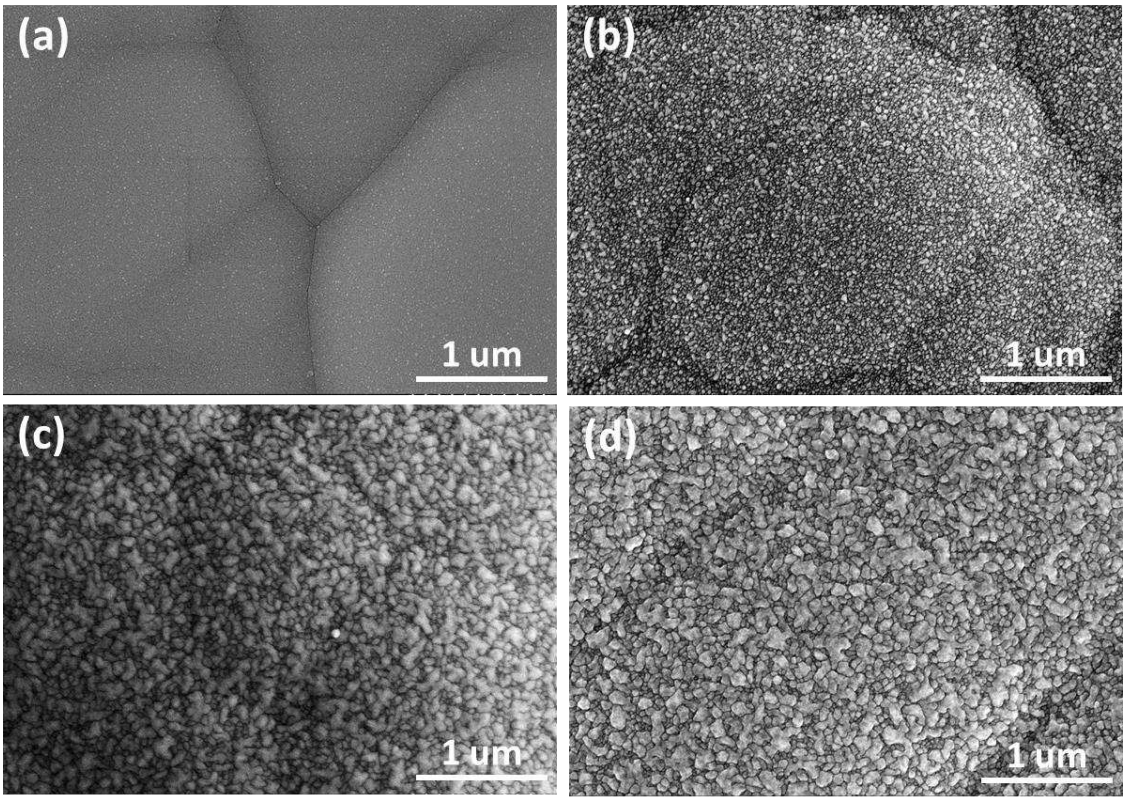
(a)
1 um
(b)
1 um
(c)
1 um
(d)
1 um

Fig. 2

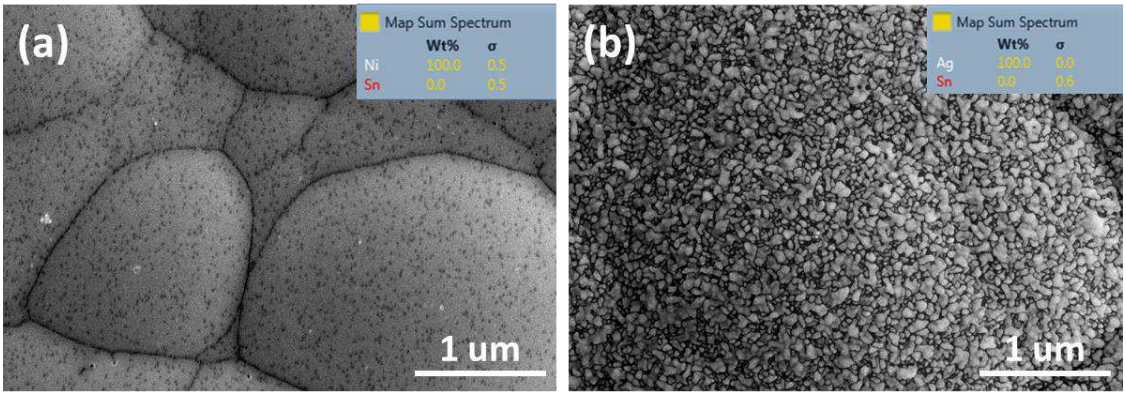
(a)
Map Sum Spectrum
Wt% σ
Ni 100.0 0.5
Sn 0.0 0.5
1 um
(b)
Map Sum Spectrum
Wt% σ
Ag 100.0 0.0
Sn 0.0 0.6
1 um

Fig. 3

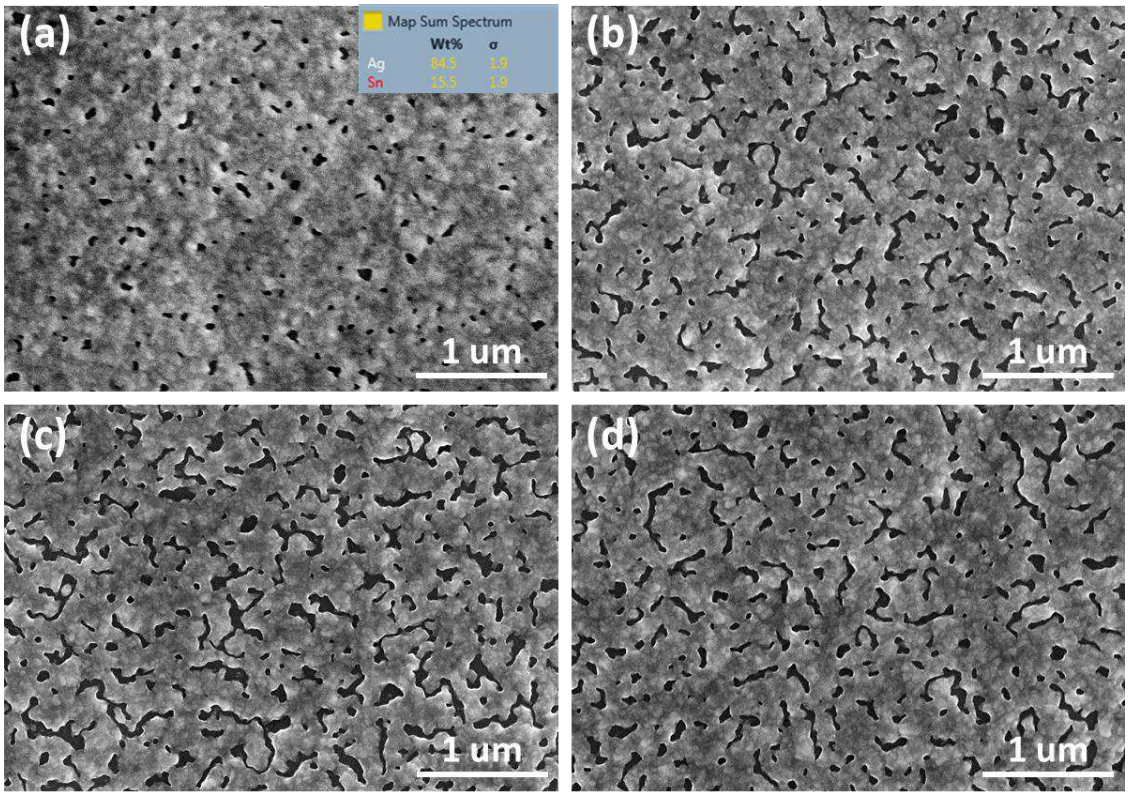


Fig. 4

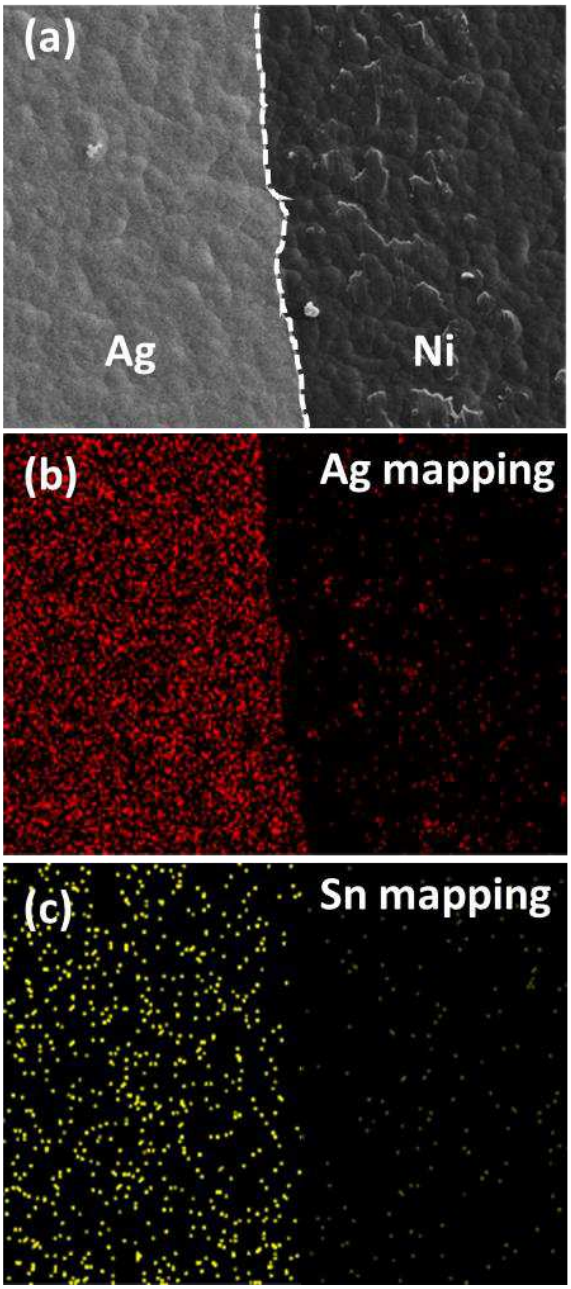


Fig. 5

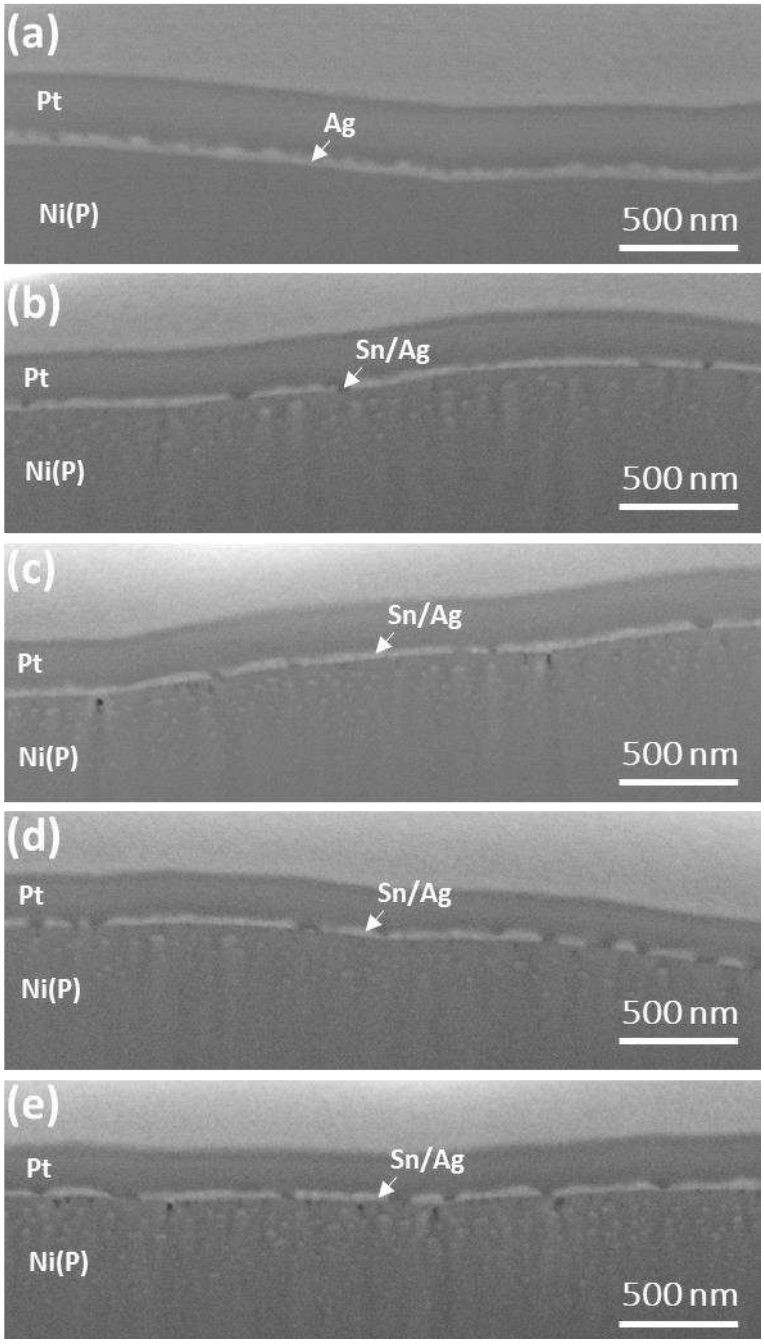
(a)
Pt
Ag
Ni(P)
500 nm
(b)
Pt
Sn/Ag
Ni(P)
500 nm
(c)
Sn/Ag
Pt
Ni(P)
500 nm
(d)
Pt
Sn/Ag
Ni(P)
500 nm
(e)
Pt
Sn/Ag
Ni(P)
500 nm

Fig. 6

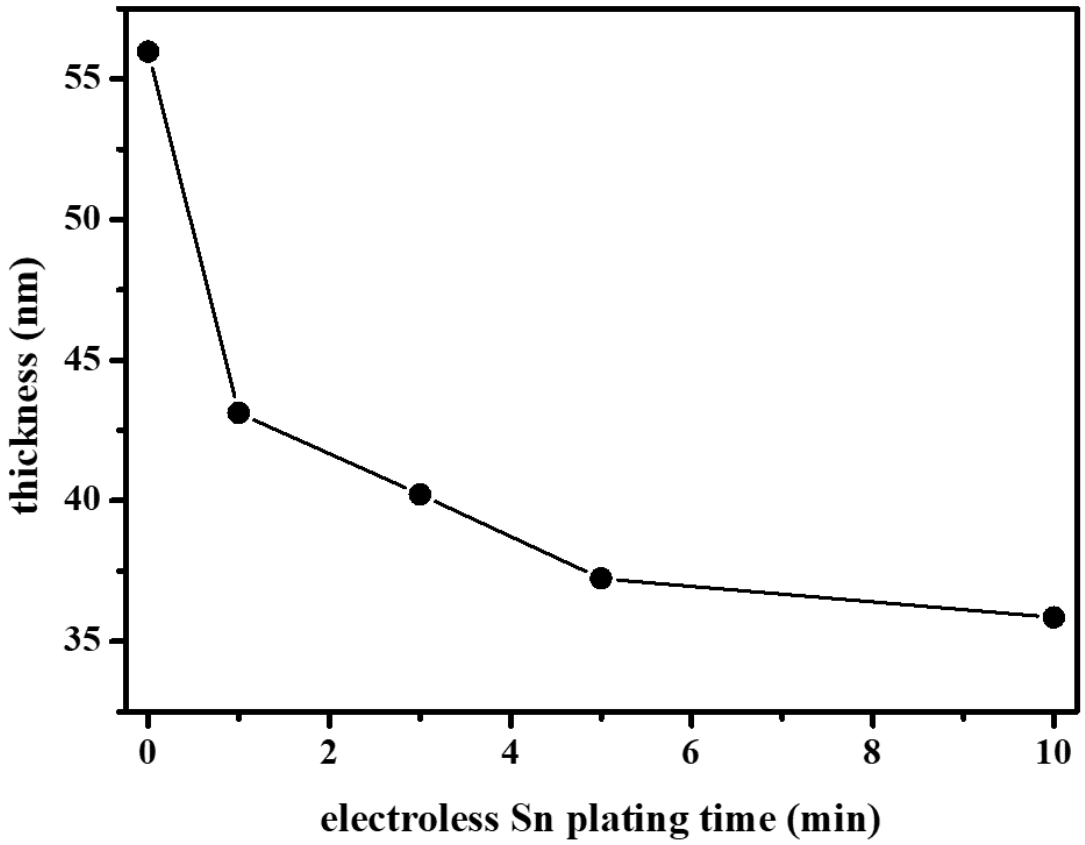
thickness (nm)
55
50
45
40
35
0
2
4
6
8
10
electroless Sn plating time (min)

Fig. 7

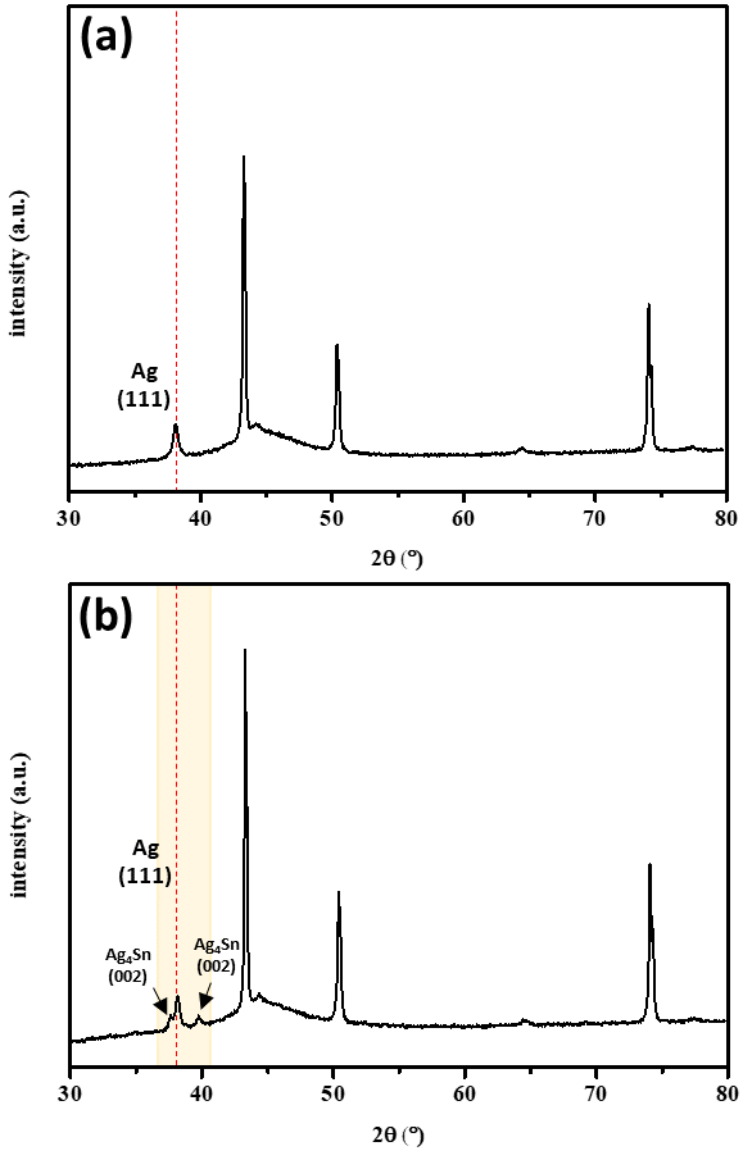
(a)
intensity (a.u.)
Ag
(111)
30
40
50
60
70
80
2θ (°)
(b)
intensity (a.u.)
Ag
(111)
Ag4Sn
(002)
Ag4Sn
(002)
30
40
50
60
70
80
2θ (°)

Fig. 8

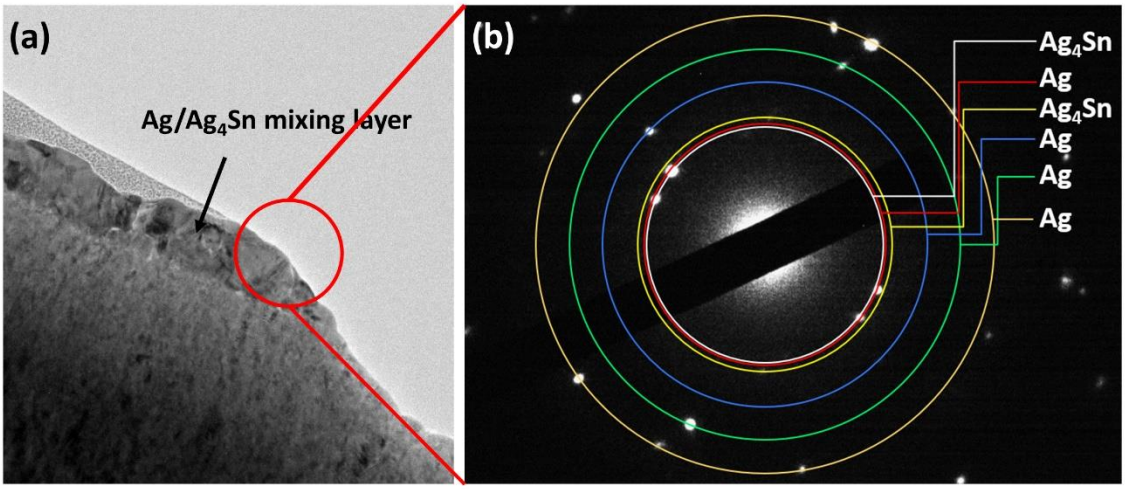
(a)
Ag/Ag4Sn mixing layer
(b)
Ag4Sn
Ag
Ag4Sn
Ag
Ag
Ag

Fig. 9

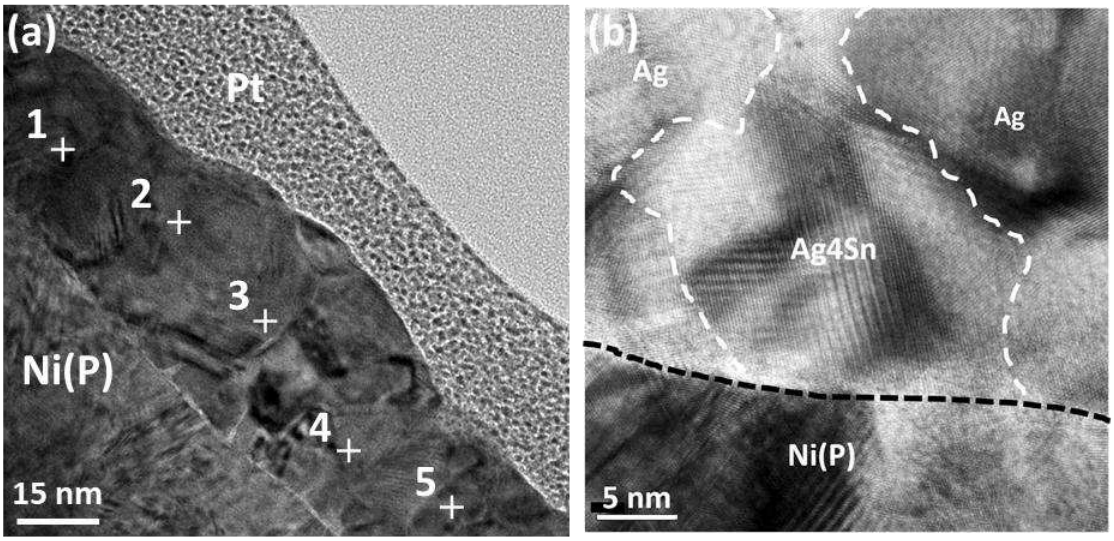
(a)
Pt
1
2
3
Ni(P)
4
5
15 nm
(b)
Ag
Ag
Ag4Sn
Ni(P)
5 nm

Fig. 10

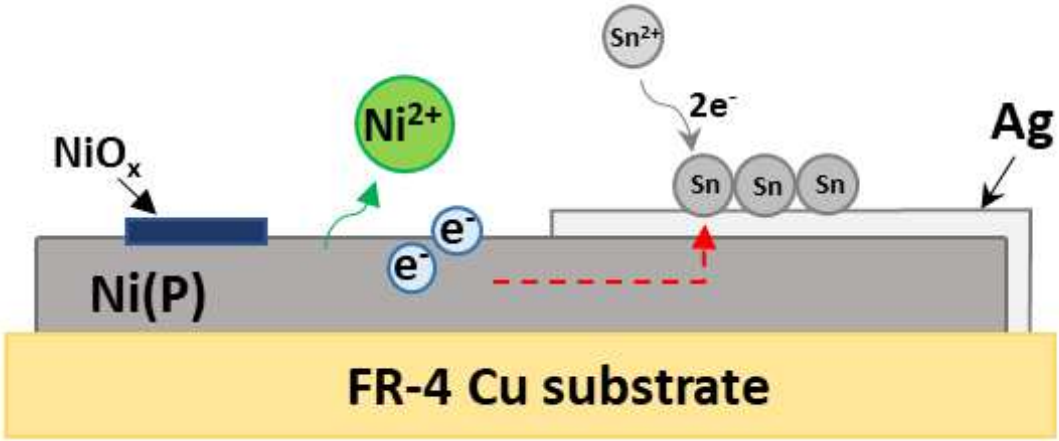
Sn2+
2e-
Ni2+
NiOx
Ag
Sn
Sn
Sn
e-
e-
Ni(P)
FR-4 Cu substrate

Fig. 11

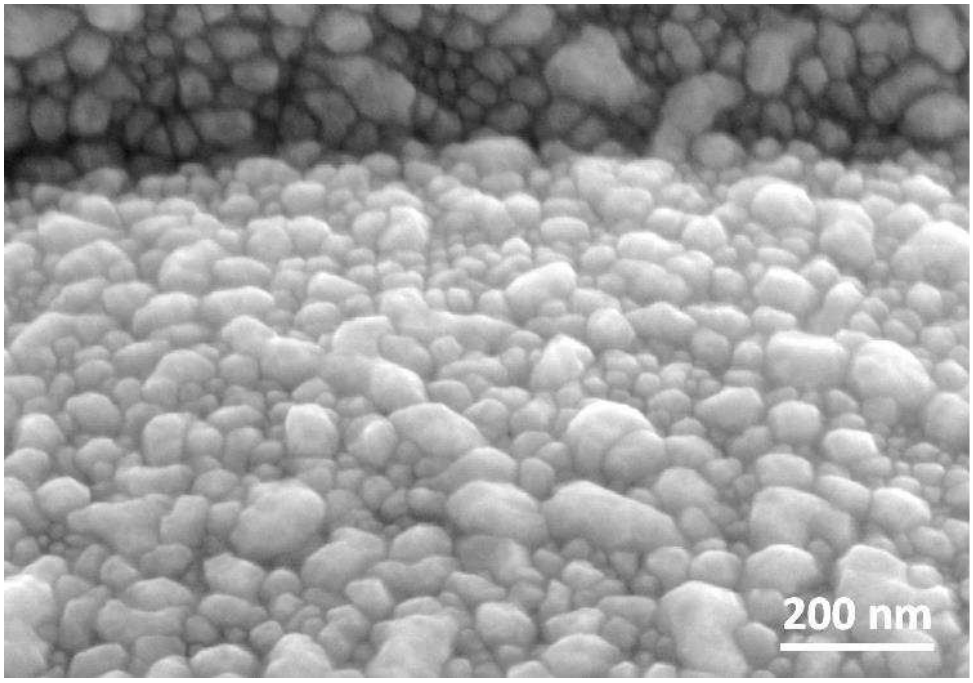


Fig. 12

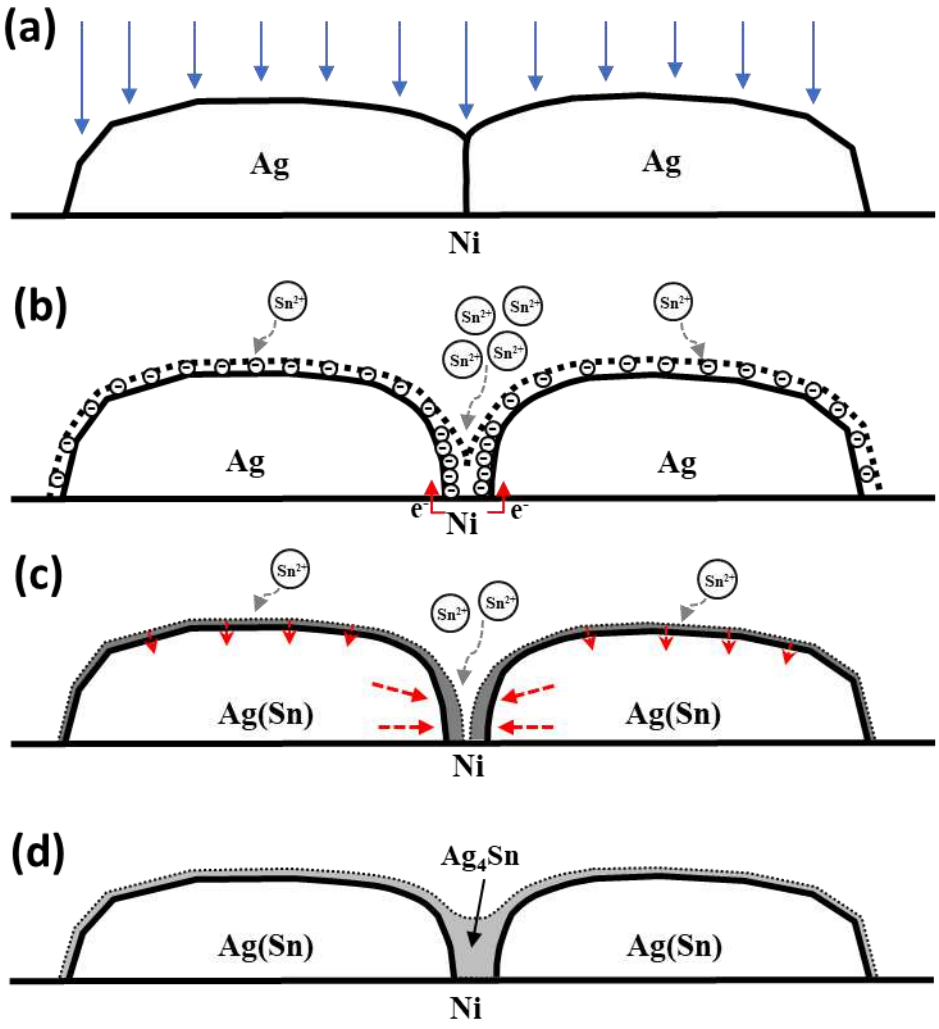


Fig. 13

Table. 1

| Position | Sn content (wt.%) |
|---|---|
| 1 | 2.49 |
| 2 | 3.91 |
| 3 | 2.76 |
| 4 | 3.41 |
| 5 | 3.99 |

**Citation**


1. PALANIAPPA, M.; SESHADRI, S. K. Friction and wear behavior of electroless Ni–P and Ni–W–P alloy coatings. Wear, 2008, 265.5-6: 735-740.
2. YAN, M.; YING, H. G.; MA, T. Y. Improved microhardness and wear resistance of the as-deposited electroless Ni–P coating. Surface and Coatings Technology, 2008, 202.24: 5909-5913.
3. LIN, Yung-Chi; WANG, Kai-Jheng; DUH, Jenq-Gong. Detailed phase evolution of a phosphorous-rich layer and formation of the Ni-Sn-P compound in Sn-Ag-Cu/electroplated Ni-P solder joints. Journal of Electronic Materials, 2010, 39.3: 283-294.
4. ZHU, W. H., et al. Drop reliability study of PBGA assemblies with SAC305, SAC105 and SAC105-Ni solder ball on Cu-OSP and ENIG surface finish. In: 2008 58th Electronic Components and Technology Conference. IEEE, 2008. p. 1667-1672.
5. SNUGOVSKY, PAMRP; ARROWSMITH, P.; ROMANSKY, M. Electroless Ni/immersion Au interconnects: investigation of black pad in wire bonds and solder joints. Journal of Electronic Materials, 2001, 30.9: 1262-1270.
6. MEDGYES, Bálint, et al. Electrochemical migration of Sn and Ag in NaCl environment. In: 2016 IEEE 22nd International Symposium for Design and Technology in Electronic Packaging (SIITME). IEEE, 2016. p. 274-278.
7. AMLI, Siti Farahnabilah Muhd, et al. Effect of surface finish on the wettability and electrical resistivity of Sn-3.0 Ag-0.5 Cu solder. In: IOP Conference Series: Materials Science and Engineering. IOP Publishing, 2019. p. 012029.
8. KURE-CHU, Song-Zhu; YASHIRO, Hitoshi. Corrosion Resistance of Multilayered Sn/Ag3Sn Films Electroplated on Cu Alloys for Highly Reliable Automotive Connectors. Journal of the Electrochemical Society, 2014, 161.10:

C441.

9. TAKENAKA, Toshio; KAJIHARA, Masanori. Fast penetration of Sn into Ag by diffusion induced recrystallization. Materials Transactions, 2006, 47.3: 822-828.
10. LIS, Adrian, et al. Early stage growth characteristics of Ag3Sn intermetallic compounds during solid–solid and solid–liquid reactions in the Ag–Sn interlayer system: Experiments and simulations. Journal of Alloys and Compounds, 2014, 617: 763-773.
11. JO, Yun Hwan, et al. Synthesis and characterization of highly conductive Sn–Ag bimetallic nanoparticles for printed electronics. Journal of Nanoparticle Research, 2012, 14.4: 782.
12. GOLLAS, Bernhard, et al. Thin layer in situ XRD of electrodeposited Ag/Sn and Ag/In for low-temperature isothermal diffusion soldering. Intermetallics, 2008, 16.8: 962-968.
13. ROSSI, P. J., et al. Dependence of intermetallic compound formation on the sublayer stacking sequence in Ag–Sn bilayer thin films. Acta Materialia, 2016, 103: 174-183.
14. WRONKOWSKA, A. A., et al. Spectroscopic ellipsometry study of the dielectric response of Au–In and Ag–Sn thin-film couples. Applied Surface Science, 2010, 256.15: 4839-4844.
15. YUANTAO, Ning; XINMING, Zhou. Metastable extension of solid solubility of alloying elements in silver. Journal of Alloys and Compounds, 1992, 182.1: 131-144.
16. KARAKAYA, I.; THOMPSON, W. T. The Ag-Sn (silver-tin) system. Bulletin of Alloy Phase Diagrams, 1987, 8.4: 340-347.
17. THERON, C. C., et al. First phase formation at interfaces: Comparison between Walser-Bené and effective heat of formation model. Materials Chemistry and

Physics, 1996, 46.2-3: 238-247.

18. PRETORIUS, René, et al. Compound phase formation in thin film structures. Critical reviews in Solid State and Materials Sciences, 1999, 24.1: 1-62.
19. FLANDORFER, H., et al. Interfaces in lead-free solder alloys: enthalpy of formation of binary Ag–Sn, Cu–Sn and Ni–Sn intermetallic compounds. Thermochimica Acta, 2007, 459.1-2: 34-39.
20. HUBBARD, Camden R.; SNYDER, Robert L. RIR-measurement and use in quantitative XRD. Powder Diffraction, 1988, 3.2: 74-77.
21. ABBOTT, J. R.; MILLER, D. R.; NETHERWAY, D. J. Plastic deformation of ß and γ phase silver-tin alloys. Journal of Materials Science, 1984, 19.10: 3255-3265.
22. DYSON, Brian F. Diffusion of gold and silver in tin single crystals. Journal of Applied Physics, 1966, 37.6: 2375-2377.

# Figures

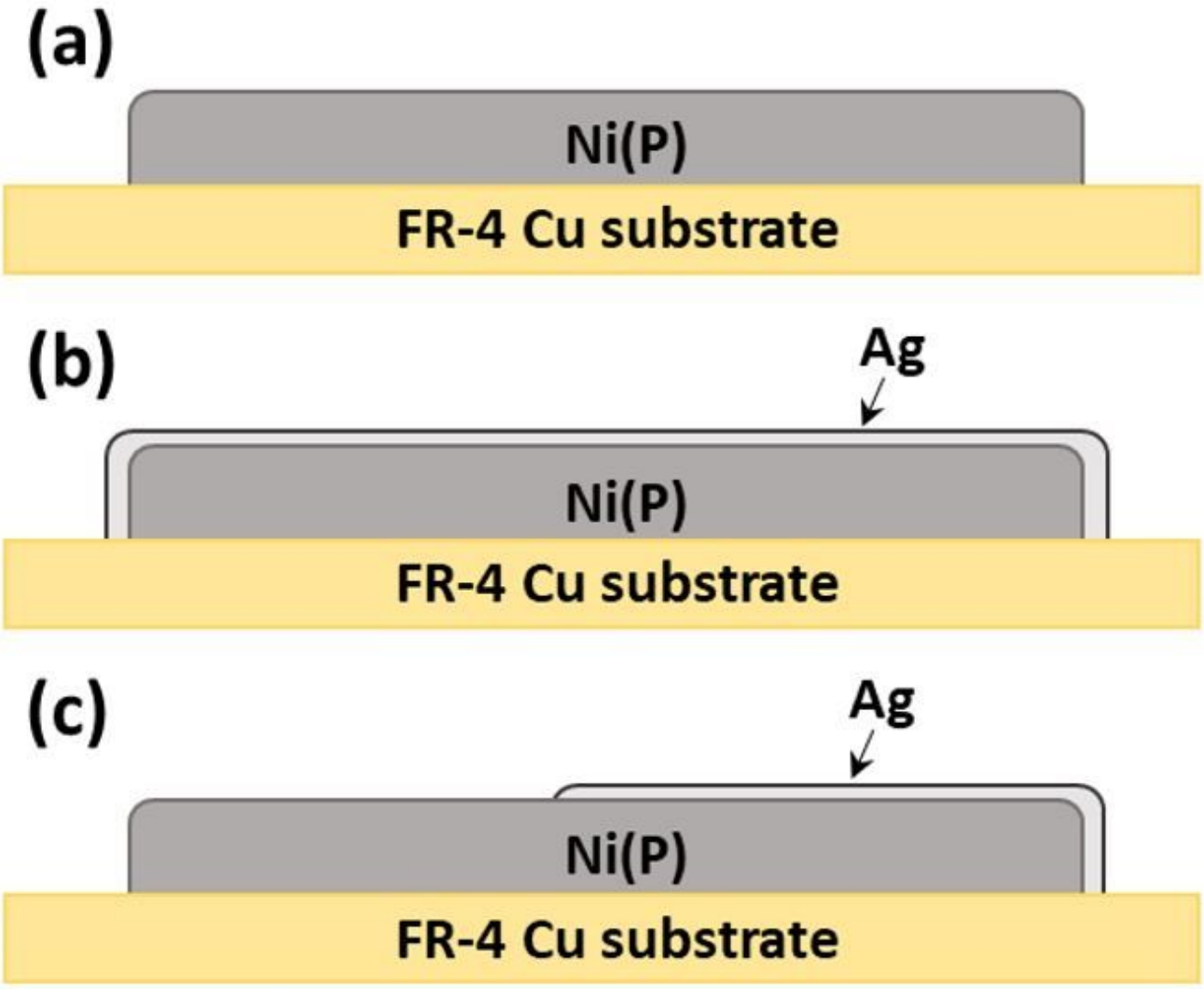


**Figure 1**

Schematic of (a) electroless EN substrate, (b) ENIS, and (c) EN-ENIS specimens

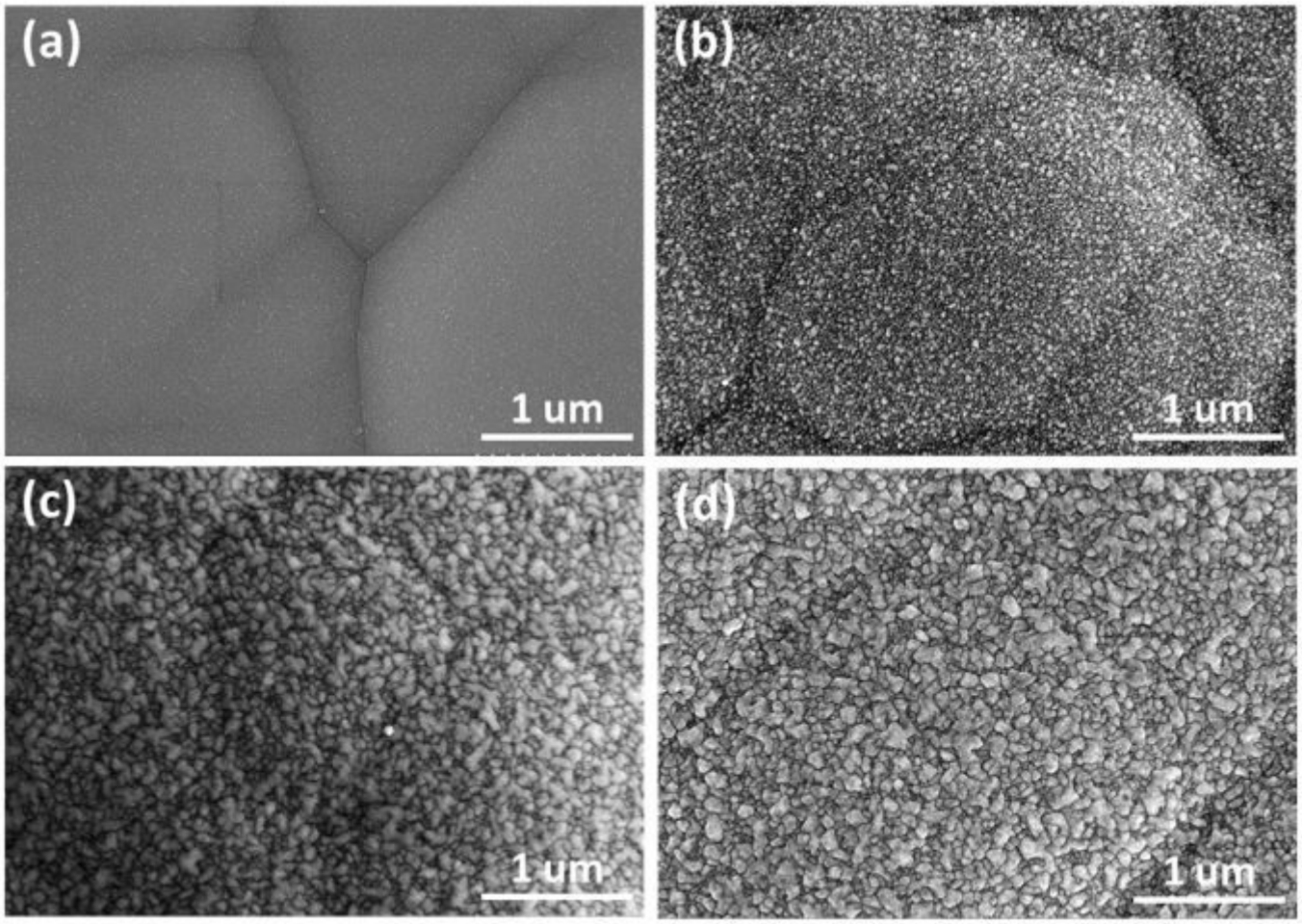


**Figure 2**

SEM images of (a) electroless EN, (b) 15-s-immersion Ag, (c) 45-s-immersion Ag, and (d) 90-s-immersion Ag

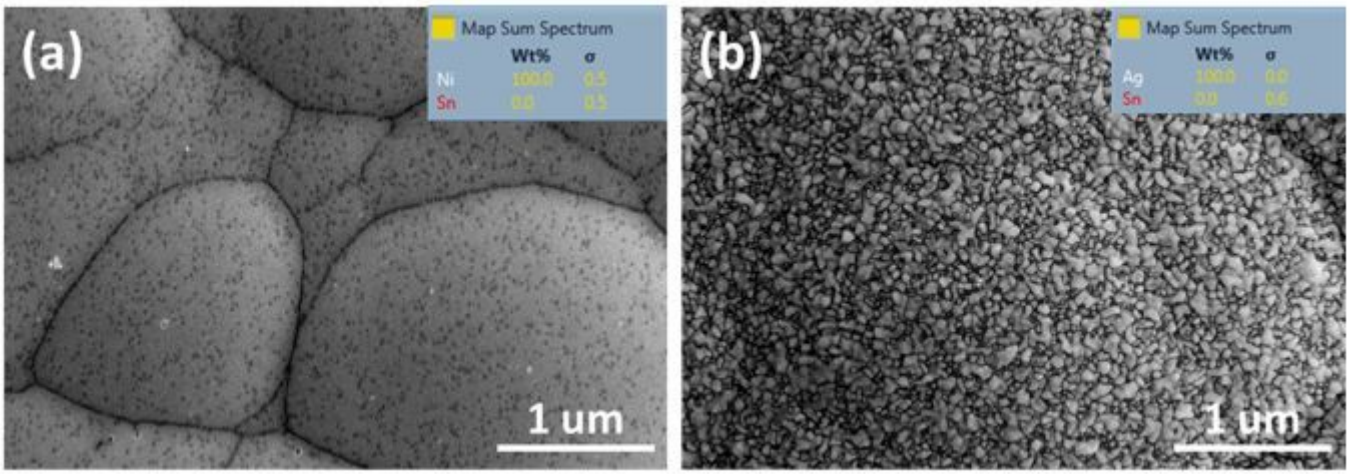


**Figure 3**

Immersion Sn on (a) EN substrate and (b) ENIS specimens

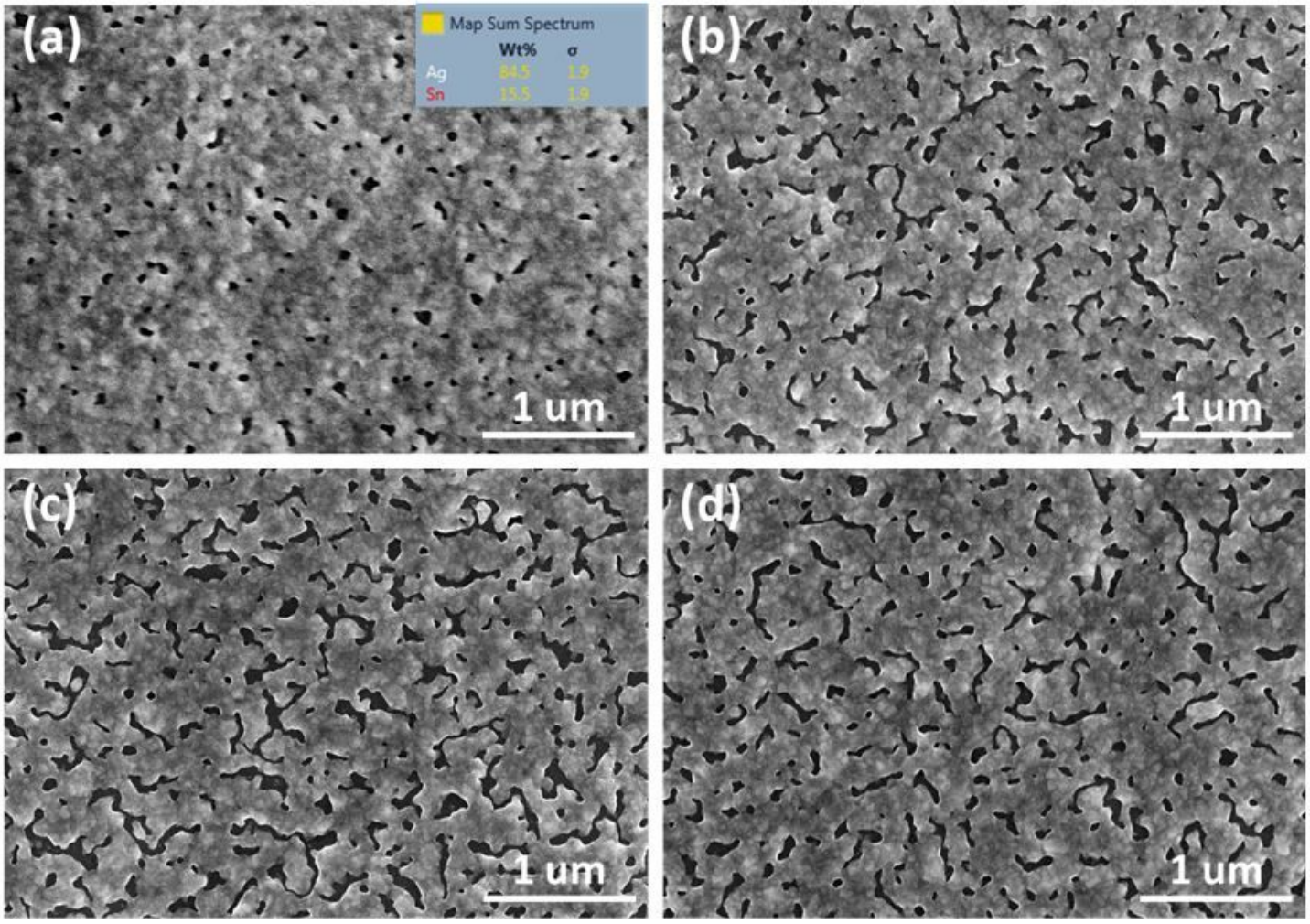


**Figure 4**

Immersion Sn with different plating times: (a) 1, (b) 3, (c) 5, and (d) 10 min

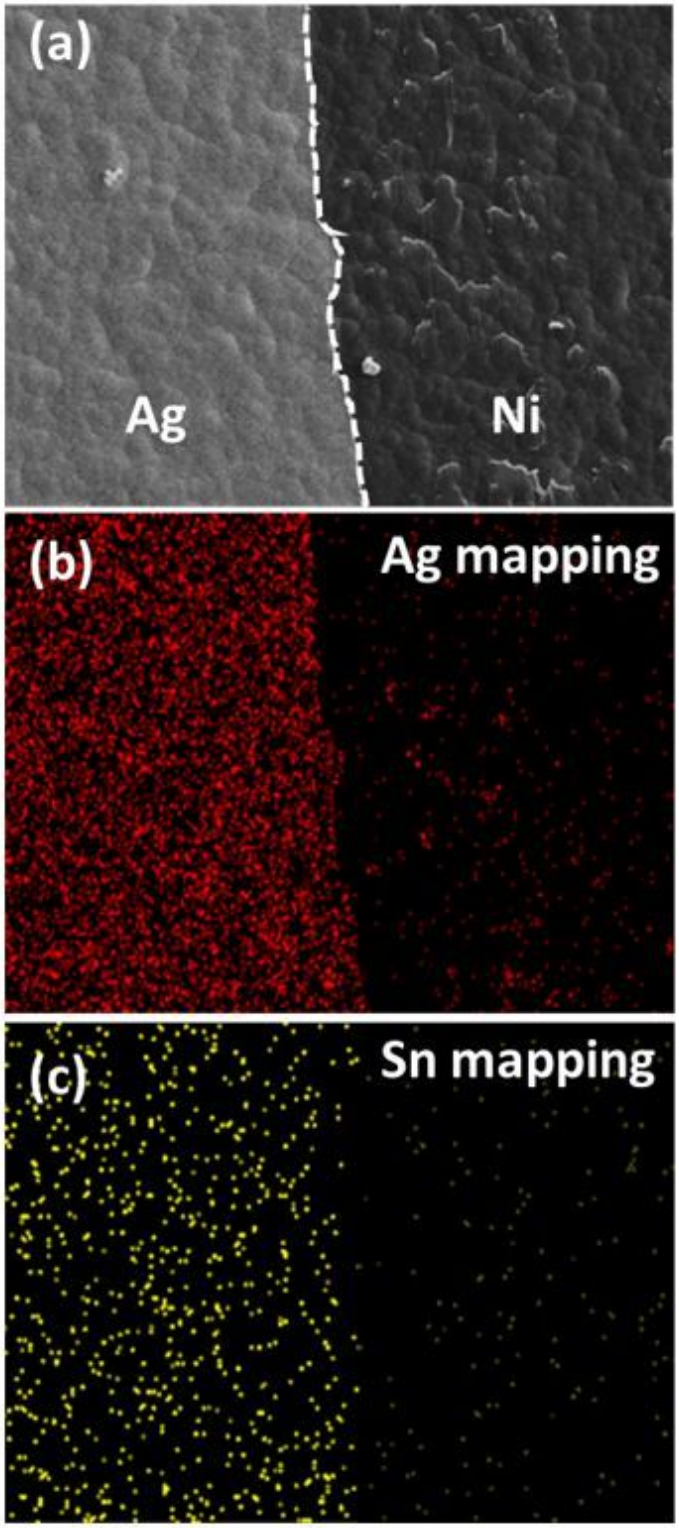


**Figure 5**

(a) SEM image of the interface between EN and ENIS, and EDS mapping of the selected region showing elemental distribution of (b) Ag and (c) Sn

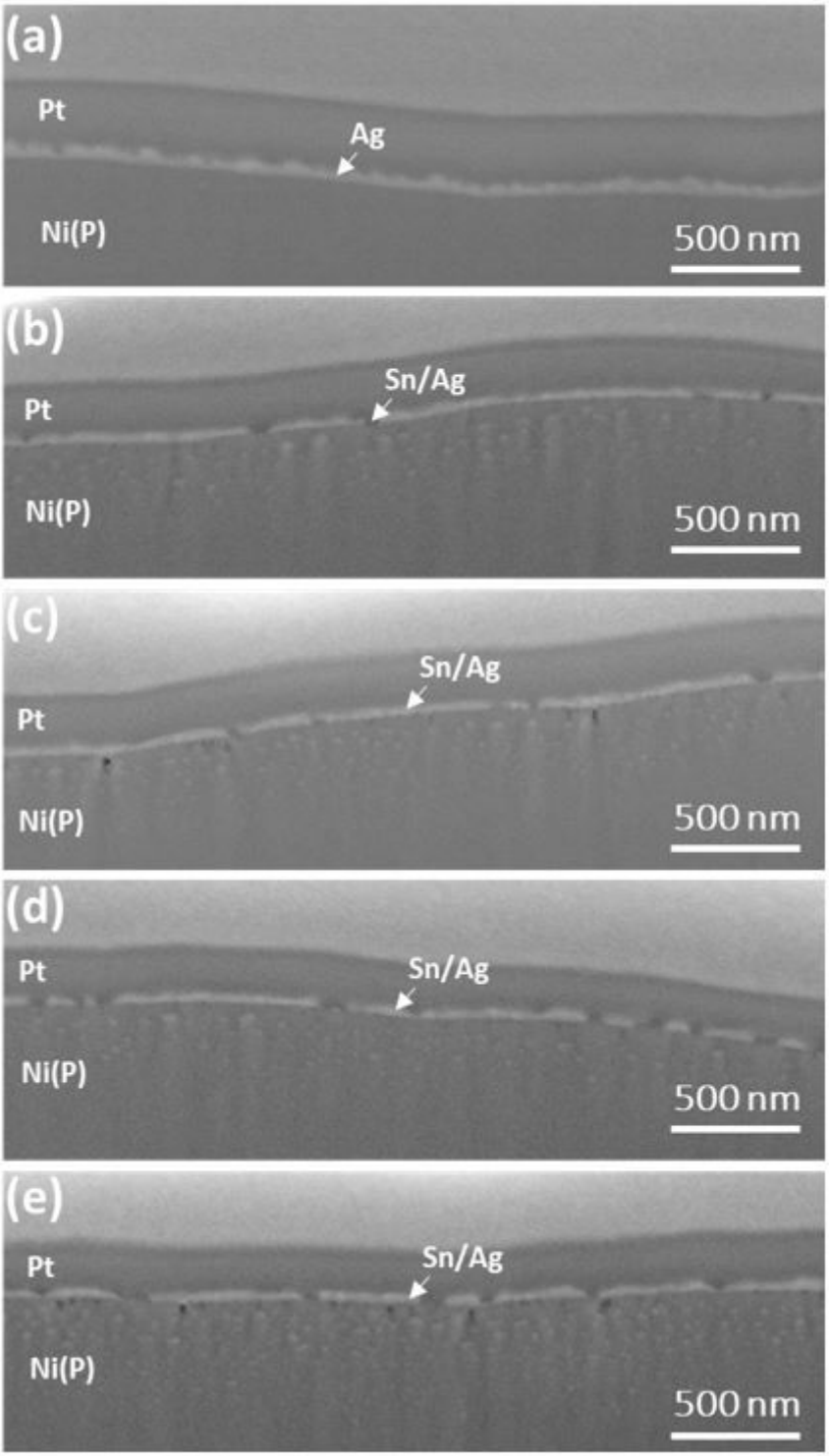


**Figure 6**

Cross-section of the metallic layer with different Sn plating times: (a) as-plated Ag; and immersion Sn plating time for (b) 1, (c) 3, (d) 5, and (e) 10 min

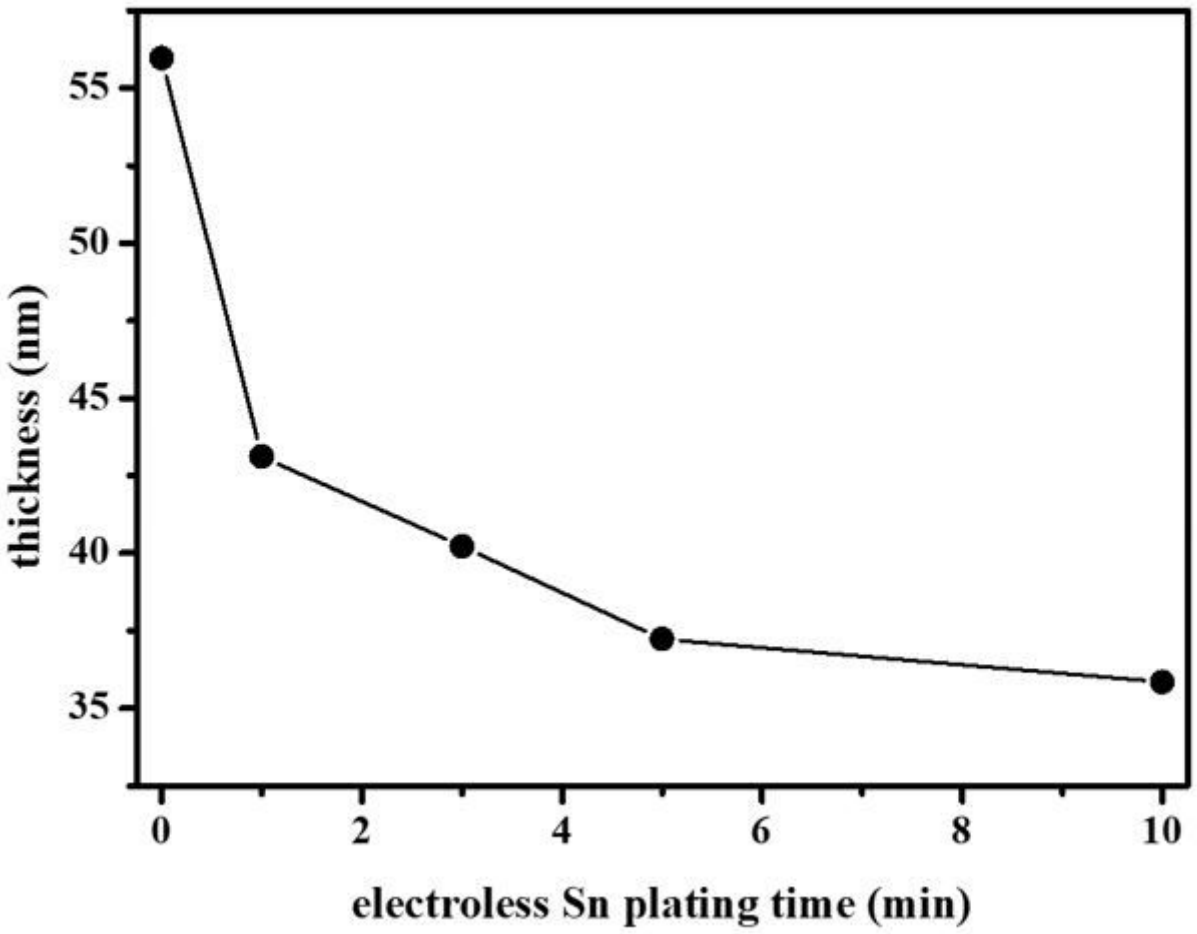


Figure 7

Variation in metallic layer thickness with immersion time

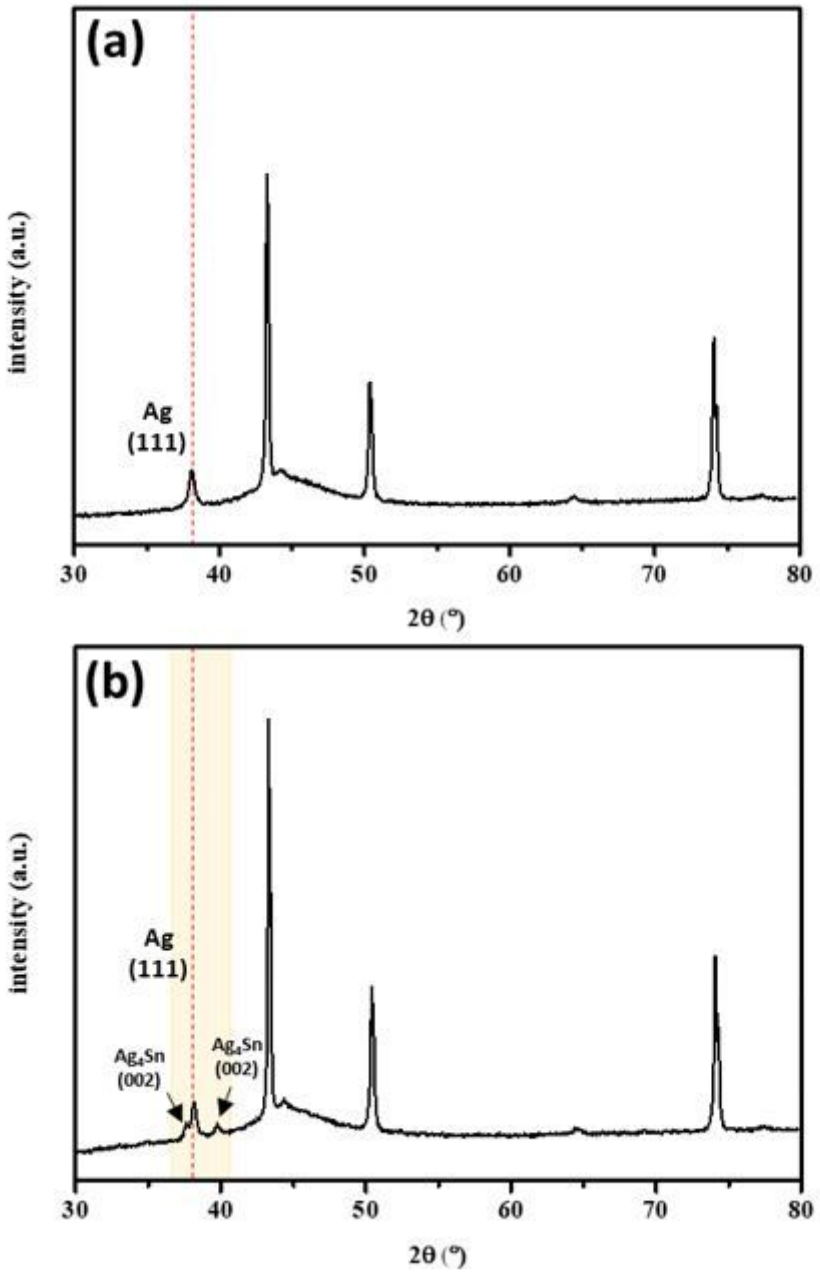


## Figure 8

XRD diffraction pattern of (a) as-deposited immersion Ag layer and (b) metallic layer after immersion Sn layer

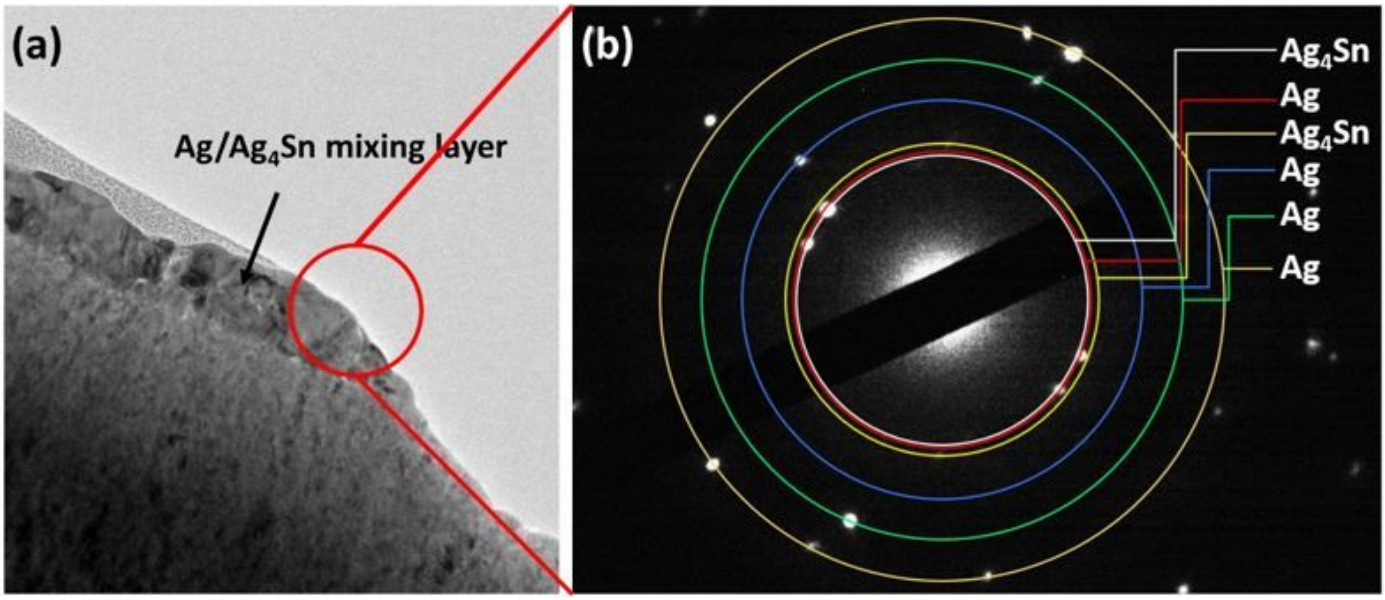


**Figure 9**

HR-TEM selected-area diffraction of metallic layer

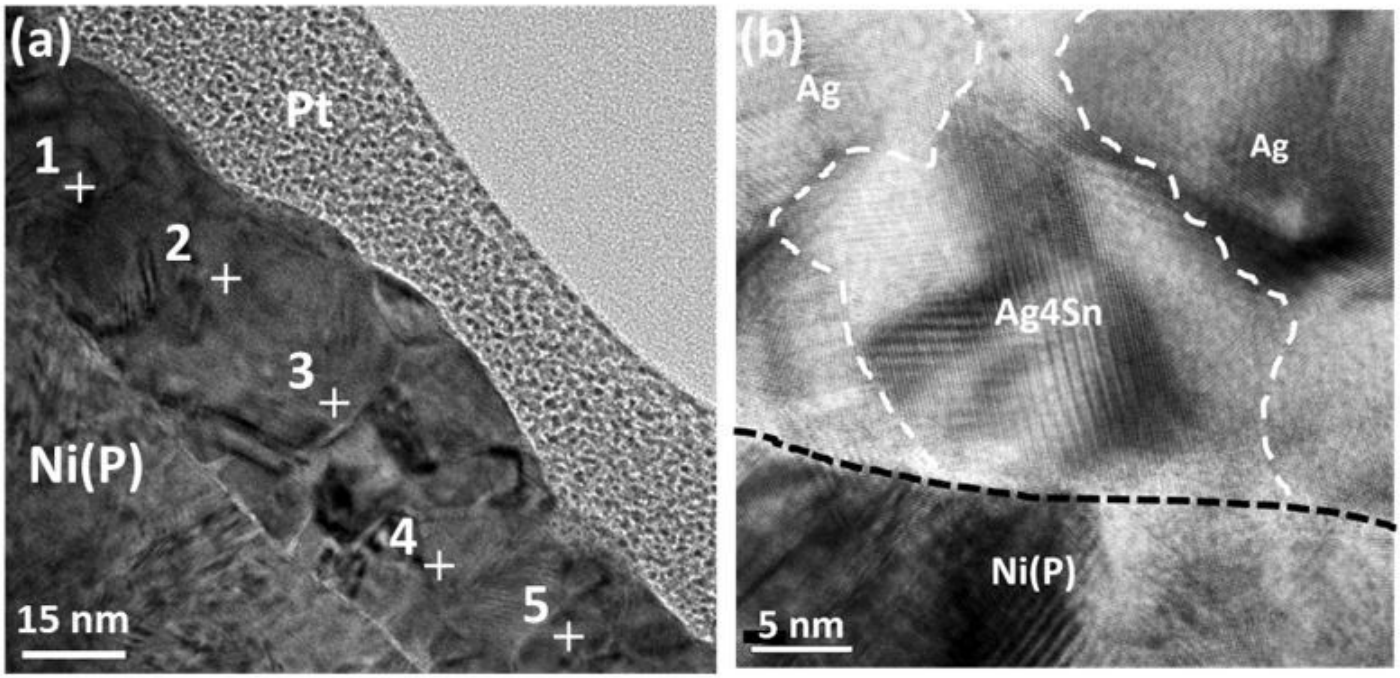


**Figure 10**

HR-TEM image of metallic layer

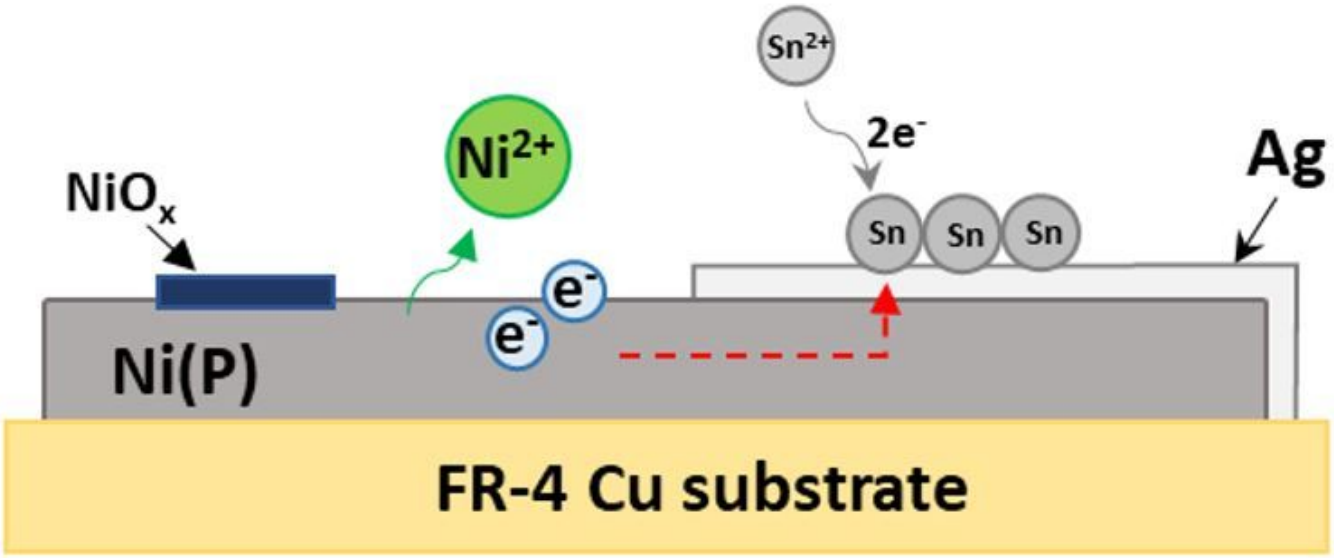


Figure 11

Schematic of nanogalvanic cell formation in EN-ENIS with immersion Sn plating solution

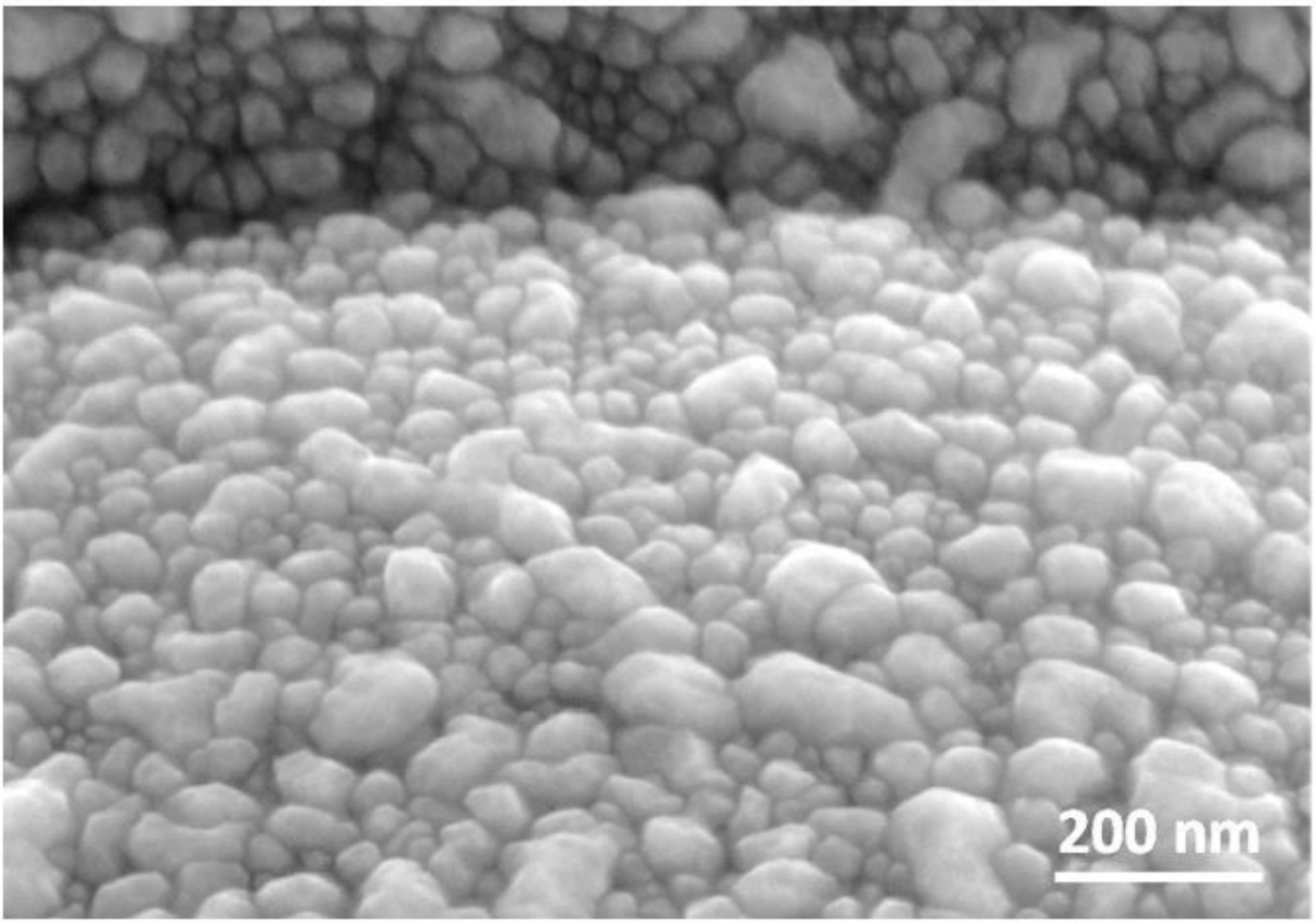


Figure 12

SEM images of Ag clusters with tilt angle

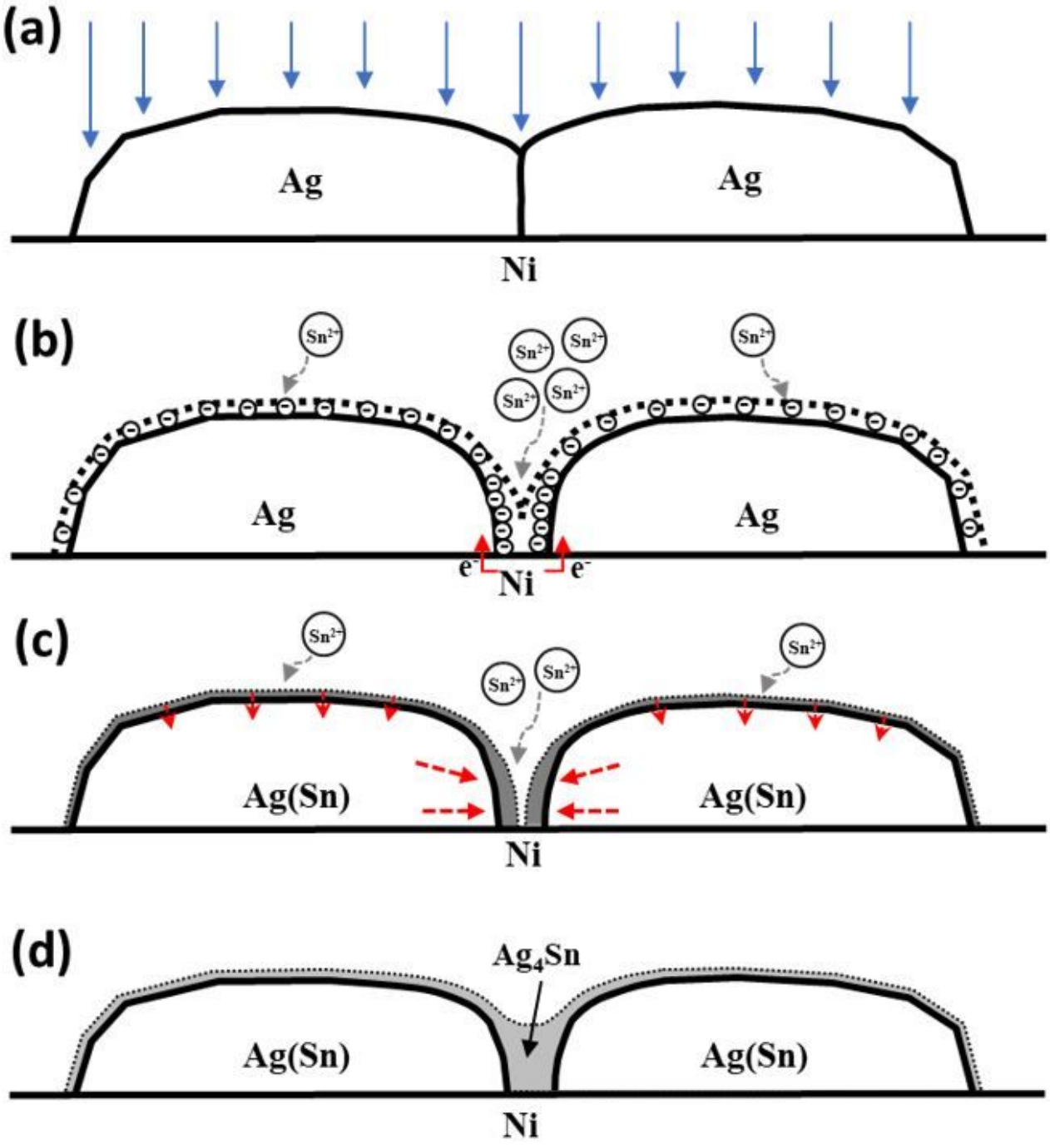


**Figure 13**

Schematic of Sn diffusion into Ag clusters with Ag4Sn formation along Ag grain boundaries